

# Molecular Asymmetry and Optical Cycling: Laser Cooling Asymmetric Top Molecules

Benjamin L. Augenbraun,<sup>1,2,\*</sup> John M. Doyle,<sup>1,2</sup> Tanya Zelevinsky,<sup>3</sup> and Ivan Kozyryev<sup>3,†</sup>

<sup>1</sup>*Department of Physics, Harvard University, Cambridge, MA 02138, USA*

<sup>2</sup>*Harvard-MIT Center for Ultracold Atoms, Cambridge, MA 02138, USA*

<sup>3</sup>*Department of Physics, Columbia University, New York, NY 10027, USA*

(Dated: December 21, 2024)

We present a practical roadmap to achieve optical cycling and laser cooling of asymmetric top molecules (ATMs). Our theoretical analysis describes how reduced molecular symmetry, as compared to diatomic and symmetric non-linear molecules, plays a role in photon scattering. We present methods to circumvent limitations on rapid photon cycling in these systems. We calculate vibrational branching ratios for a diverse set of asymmetric top molecules and find that many species within a broad class of molecules can be effectively cooled with a manageable number of lasers. We also describe methods to achieve rotationally closed optical cycles in ATMs. Despite significant structural complexity, laser cooling can be made effective using extensions of the current techniques used for linear molecules. Potential scientific impacts of laser-cooled ATMs span frontiers in controlled chemistry, quantum simulation, and searches for physics beyond the Standard Model.

## I. INTRODUCTION

Deviations from perfect symmetry play an important role in Nature at a variety of spatial and temporal scales [1, 2], ranging from the interactions of subatomic particles [3, 4] to key biological processes like embryonic laterality [5, 6]. Many important biochemical processes in the human body involve chiral molecules, which are necessarily asymmetric tops [7, 8]. Despite their fundamental importance in other branches of science, asymmetric top molecules (ATMs, molecules with three distinct moments of inertia) have not been put under full quantum control. The traditional tools used to manipulate atomic and molecular samples with exquisite precision generally break down for ATMs due to intrinsic structural complexity.

Highly symmetric, linear molecules have been brought under quantum control via recent advances producing laser-cooled molecules in the  $\mu\text{K}$  regime. This has spurred progress in such diverse fields as ultracold chemistry [9–11], quantum simulation of strongly correlated systems [12], and precision tests of fundamental physics [13, 14]. In many cases, the rich variety of structures afforded by many molecules (e.g., large, permanent body-frame electric dipole moments and closely-spaced pairs of levels with opposite parity) conveys fundamental advantages over atomic alternatives. Direct laser cooling of molecules is a new, important tool for reaching the ultracold regime and achieving full control over the quantum state of the molecule. Furthermore, cooling allows for the long interaction times required to exploit these structures.<sup>1</sup> SrF [16, 17], CaF [18–21], and YO [22] have been directly laser-cooled, trapped, and had their

quantum states detected with near unit efficiency. The linear triatomic molecules SrOH [23, 24], YbOH [25], and CaOH [26] have been laser cooled in one dimension, the first step to full quantum control.

Direct laser cooling requires a closed optical cycling transition such that  $> 10^4$  photons may be scattered using a reasonable number of lasers and without significant loss to dark manifolds of states [27]. To date, only linear molecules have been directly laser cooled. The high degree of symmetry in these molecules greatly restricts the decay channels that could remove a molecule from the optical cycle. Extending the technique to *asymmetric* molecules necessarily involves removing these restrictions. While Isaev and Berger previously performed *ab initio* estimates of the vibrational branching ratios for the chiral ATM MgCHDT [28], to date there has been no complete description of general methods to directly laser cool and trap ATMs. It has not previously been clear how the reduced symmetry of ATMs would affect optical cycling, or even if full laser cooling of asymmetric species would be possible.

Although potentially challenging to produce, ultracold ATMs would offer many qualitatively unique features useful for a broad range of science. For example, ATMs can have up to three permanent dipole moments that could conceivably be controlled independently, a feature never present in higher symmetry species. Low-lying states with very long radiative lifetimes and dipole moments  $\sim 5$  D have been observed, promising strong molecule-molecule coupling [29]. In addition, asymmetric molecular structures often arise when various chemically interesting ligands (e.g.,  $\text{NH}_2$ ,  $\text{SH}$ ,  $\text{OC}_2\text{H}_5$ ,  $\text{OCH}(\text{CH}_3)_2$ ,  $\text{C}_4\text{H}_5\text{N}$ , etc.) are bonded to the optical cycling center atom. Finally, chiral molecules are, by necessity, ATMs. The determination of a general method to laser cool

\* [augenbraun@g.harvard.edu](mailto:augenbraun@g.harvard.edu)

† [ik2452@columbia.edu](mailto:ik2452@columbia.edu)

<sup>1</sup> The technique of optoelectric Sisyphus cooling [15] is a complementary method to cool polyatomic molecules. However, it relies on neither directional momentum exchange between laser fields

and molecules nor cycling optical photons, and is therefore orthogonal to the ideas described in this work.

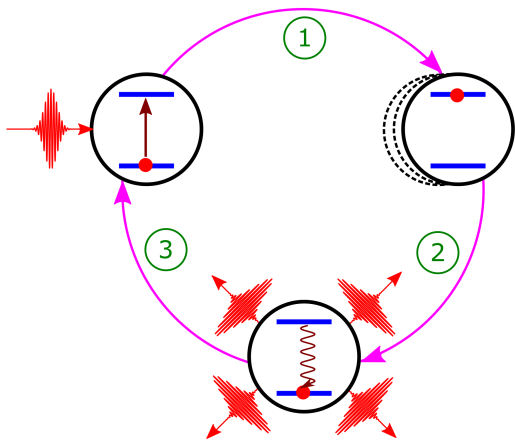


FIG. 1. Schematic diagram of optical cycling in an ideal two-level system. Repetition of steps 1-3 are required to achieve radiative laser cooling: 1. directional photon absorption, 2. isotropic spontaneous emission, and 3. decay to the initial quantum level. The complex structure of molecules can interrupt this cycle, e.g. by the addition of multiple decay pathways during step 3.

ATMs— allowing a ligand to be chosen primarily for its targetted utility rather than technological accessibility— could open up new avenues in fields including quantum information/simulation, ultracold chemistry, and precision measurements (see Sec. IV).

In this paper, we demonstrate that a general class of ATMs is amenable to laser cooling and trapping techniques. We focus on species of the form M-L, comprising an alkaline-earth atom (M) that is ionically and monovalently bonded to an electronegative ligand (L). In this case the metal-centered unpaired valence electron is expected to act somewhat independently of the bond, leading to good optical cycling properties [30, 31]. We present calculations of the vibrational branching ratios in these molecules, demonstrating that with only a few repumping lasers one may scatter enough photons to slow, trap, and cool the molecules to the Doppler limit. Once at that temperature, these molecules will be generically amenable to sub-Doppler techniques, allowing access to the  $\mu\text{K}$  regime. Crucially, we describe how, despite the complex rotational structure in these asymmetric tops, a simple laser cooling scheme may be constructed that limits rotational branching to an easily repumped manifold of states. Using available spectroscopic data and new *ab initio* quantum chemistry calculations we discover that, surprisingly, in many cases the required experimental complexity is not significantly greater than that encountered with linear polyatomic molecules. Finally, we elaborate on some applications of trapped, ultracold ATMs that our work opens.

## II. ACHIEVING PHOTON CYCLING

Photon cycling, the repeated absorption and emission of photons, is a fundamental necessity to laser cooling (see Fig. 1). In this section we discuss how the achievement of photon cycling is complicated by molecular structure. We present here techniques to overcome these complications.

Working within the Born-Oppenheimer approximation, we separate the discussion of electronic, vibrational, and rotational excitations. The possibility of Born-Oppenheimer approximation breakdown and its challenges are discussed in App. A.

Laser cooling relies on photon cycling to generate dissipative forces [27, 32]. Typically  $\sim 10^4 - 10^5$  photon scatters are necessary to apply sufficient force for slowing, cooling, and trapping. This requires an excited state that decays preferentially to one ground state, with unplugged leaks to all other (possibly metastable) levels below about 1 part in  $10^4$ . In the case of atoms, the simplest with this electronic structure are alkali or alkaline-earth (AE) atoms with one or two valence electrons in  $s$  orbitals. Electronic branching is then limited, or wholly eliminated, so that repumping from “dark” levels is easily achieved with at most a few additional laser frequencies. In the case of molecules, certain classes with  $^2\Sigma$  ground states have been found to be favorable to laser cooling due to their single valence electron in a metal-centered  $s\sigma$  orbital [27, 32]. This leads to a simple electronic structure that closely resembles that of alkali metal atoms.

Vibrational and rotational substructure within each electronic state can be significant impediments to photon cycling in molecules. These internal degrees of freedom can change quantum number during an electronic transition, leading to the possibility of quick diffusion of population into “dark states,” i.e. states that are not coupled to the applied laser light. Molecules lost to these states will not be cooled further unless they are repumped, a task usually accomplished by application of additional laser or microwave frequencies. For linear molecules, angular momentum selection rules can eliminate losses to dark rotational levels [33]. Losses to dark vibrational states are, by contrast, always problematic due to the general lack of selection rules. Vibrational branching during an electronic decay is governed probabilistically by Franck-Condon factors (FCFs),  $q_{v',v''}$ , which characterize the overlap between excited and ground vibrational states.<sup>2</sup> Vibrational losses are highly suppressed in molecules for which the ground and excited state potential energy surfaces resemble one another, as they do for AE metal atoms monovalently and ionically bonded to an electronegative ligand ( $M^+L^-$ ). In these species, electrostatic repulsion of the  $M^+$ -centered electron by the

<sup>2</sup> Excited states are denoted by a single prime while ground states are denoted by double primes.

ligand anion induces orbital hybridization which moves the electron away from the chemical bond and strongly decouples electronic and vibrational excitations [34–36].

These ideas have led to the successful laser cooling of many AE-monofluorides and AE-monohydroxides (all linear), including SrF [16, 17, 32, 37–41], CaF [18–21, 42, 43], YbF [44], SrOH [23, 24], YbOH [25], and CaOH [26]. Isaev and Berger proposed laser cooling symmetric top molecules including CaCH<sub>3</sub> and MgCH<sub>3</sub> in 2016 [28], considering only the vibrational branching ratios. Recently, FCF calculations were reported for species with AE atoms bonded to hydrocarbon chains or fullerenes, showing that these species have vibrational branching ratios favorable for laser cooling [45]. Ref. [30] considered the issues of rotational and fine structure in symmetric, nonlinear molecules. It was found that laser cooling symmetric top molecules requires at most one additional (rotational) repumper as compared to diatomic species. For ATMs it is not obvious *a priori* that typical laser cooling techniques will be applicable because, as the degree of symmetry of a molecule is decreased, selection rules become progressively weaker; many possible rotational- and vibrational-state changing decays are allowed during an electronic transition. Any discussion of photon cycling in ATMs therefore requires careful consideration of both vibrational and rotational loss channels.

In ATMs, all three principal axes have distinct moments of inertia. These molecules can have at most twofold rotational symmetry and, formally, there can be no orbitally degenerate states in these species.<sup>3</sup> The reduced symmetry has several important consequences for laser cooling. First, mixing between electronic manifolds— especially among the closely-spaced electronically excited states  $\tilde{A}$ ,  $\tilde{B}$ , and  $\tilde{C}$ — may lead to perturbations that need to be understood and controlled in order to scatter a large number of photons. Second, vibronic selection rules that are present in the case of linear or symmetric top molecules may begin to break down. Third, the reduced symmetry requires careful consideration when attempting to construct a rotationally closed cycling transition because angular momentum selection rules are relaxed. We analyze potential loss channels related to electronic, vibrational, and rotational structure separately in the following discussion.

We consider here a very large class of molecules which has fortunately been the focus of considerable previous spectroscopic attention (making practical application in the laboratory much easier). Such species include (see Fig. 2): AE monoamides (MNH<sub>2</sub>) [46–53], hydrosulfides (MSH) [54–58], monoethoxides (MOC<sub>2</sub>H<sub>5</sub>) [59], pyrrollys (MC<sub>4</sub>H<sub>4</sub>N) [60], methylpentadienyls (MC<sub>5</sub>H<sub>4</sub>CH<sub>3</sub>) [60–62], methanethiols (MSCH<sub>3</sub>) [63], alkylamides (MNHCH<sub>3</sub>) [64], and isopropoxides (MOCH(CH<sub>3</sub>)<sub>2</sub>) [65], where M = Mg, Ca, Sr,

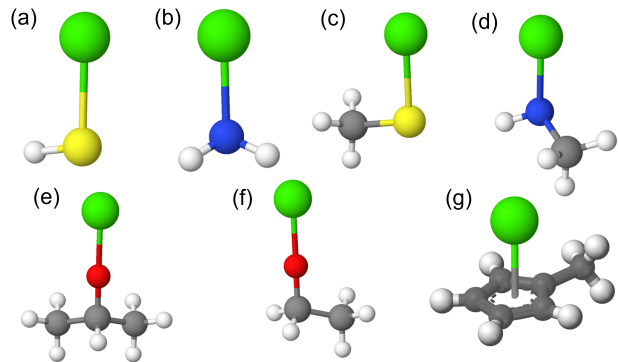


FIG. 2. Model geometries for several of the species proposed in this work. (a) MSH, (b) MNH<sub>2</sub>, (c) MSCH<sub>3</sub>, (d) MNHCH<sub>3</sub>, (e) MOCH(CH<sub>3</sub>)<sub>2</sub>, (f) MOC<sub>2</sub>H<sub>5</sub>, (g) MC<sub>5</sub>H<sub>4</sub>CH<sub>3</sub>, where M represents an alkaline-earth metal atom. Atomic species are colored according to green: alkaline-earth metal, yellow: sulfur, blue: nitrogen, red: oxygen, gray: carbon, white: hydrogen. Structures were generated using MolView [70].

or Ba.<sup>4</sup> Chiral-substituted AE-methyls (MCHDT) [66–68] and AE-methoxides (MOCHDT) [69] are also considered because the chiral methyl group will cause the three moments of inertia to differ. The wealth of spectroscopic data available for these species is essential to providing quantitative examples for the general approach to laser cooling ATMs that we describe here.

### A. Electronic Transitions

For the molecules considered in this work, the structure of the low-lying electronic states can be understood through their correlations with the electronic states of linear AE monohalides [34, 49]. A schematic energy level diagram is shown in Fig. 3. Aside from the exact symmetry species labeling, the same pattern of levels will hold for any of the ATMs considered here. As the AE-metal atom, M, approaches the ligand, L, one of the  $ns^2$  valence electrons is transferred from M to L. The electron remaining localized around M<sup>+</sup> is polarized away from the bond via orbital mixing with excited  $np$  and  $nd$  orbitals [34]. In the linear limit, the ground state,  $\tilde{X}$ , is of  $^2\Sigma^+$  symmetry while the two lowest electronically excited states are  $\tilde{A}^2\Pi$  and  $\tilde{B}^2\Sigma^+$ . As the cylindrical symmetry of the molecule is broken, the degeneracy between orbitals directed along the  $b$ - and  $c$ -axes is lifted and the  $\tilde{A}^2\Pi$  state splits in two.

<sup>3</sup> This includes point groups  $C_1$ ,  $C_i$ ,  $C_s$ ,  $C_2$ ,  $D_2$ ,  $C_{2h}$ ,  $D_{2h}$ , and  $C_{2v}$ .

<sup>4</sup> Ca and Sr-containing species have received the most attention. Some Mg and Ba-containing species have been observed, e.g. MgSH [57], BaSH [58], MgNH<sub>2</sub> [51, 52], and BaNH<sub>2</sub> [53]. Yb-containing ATMs are interesting targets due to the high- $Z$  nucleus, but have not yet been studied.

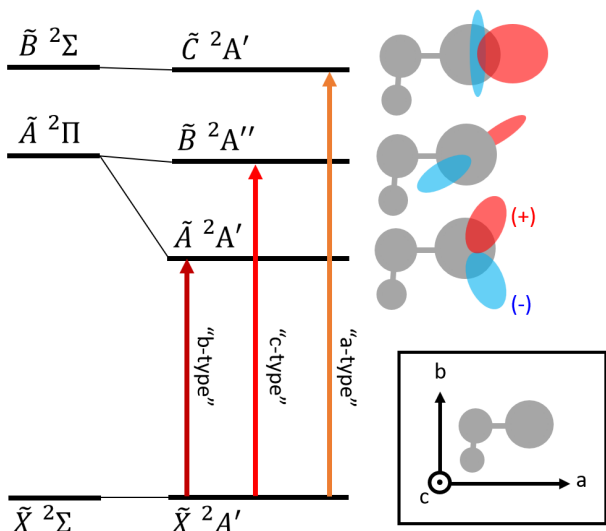


FIG. 3. Energy level diagram for species of  $C_s$  symmetry relevant to the present work, including correlations between linear (left) and asymmetric top (right) states. The asymmetry of the molecule leads to a splitting of the  ${}^2\Pi$  potential, lifting the degeneracy of the in-plane and out-of-plane orbitals. The diagram is essentially the same, aside from symmetry labeling, for other highly ionic doublet species. Optical transitions are labeled by the dominant transition dipole moment component. Schematic drawings of the orientation of the electron density are included to rationalize these assignments. Red and blue label phase of the electronic wavefunction. Inset: Principal axis system for the example species.

In general there will be four low-lying states of interest to laser cooling experiments,  $\tilde{X}{}^2A'$ ,  $\tilde{A}{}^2A'$ ,  $\tilde{B}{}^2A''$ , and  $\tilde{C}{}^2A'$  in the case of  $C_s$  symmetry. (The symmetry labeling will differ depending on the point group, but the overall structure will be similar.) For molecules of  $C_{2v}$  symmetry, like  $\text{MNH}_2$ , the principal axes of the molecule coincide with the axes along which the electronic orbitals are aligned. For molecules of lower symmetry, there will be a misalignment between the M-L bond and the primary axis along which the electronic orbitals are oriented. As will be discussed below, this angle determines to what extent the rotational selection rules expected within a given electronic transition will hold. For the species considered here, the lowest three electronically excited states can be addressed by convenient laser wavelengths ranging between 570 nm and 730 nm and have short lifetimes  $\sim 20 - 40$  ns. The visible wavelengths and large spontaneous decay rates are crucial for exerting large optical forces.

In order to understand the detailed electronic structure of laser-coolable ATMs, we have performed *ab initio* molecular structural calculations for four prototypical species:  $\text{CaOH}$  ( $C_{\infty v}$  symmetry),  $\text{CaCH}_3$  ( $C_{3v}$  symmetry),  $\text{CaNH}_2$  ( $C_{2v}$  symmetry) and  $\text{CaSH}$  ( $C_s$  symmetry). These are the four simplest species within each symmetry group considered. Figure 4 provides a com-

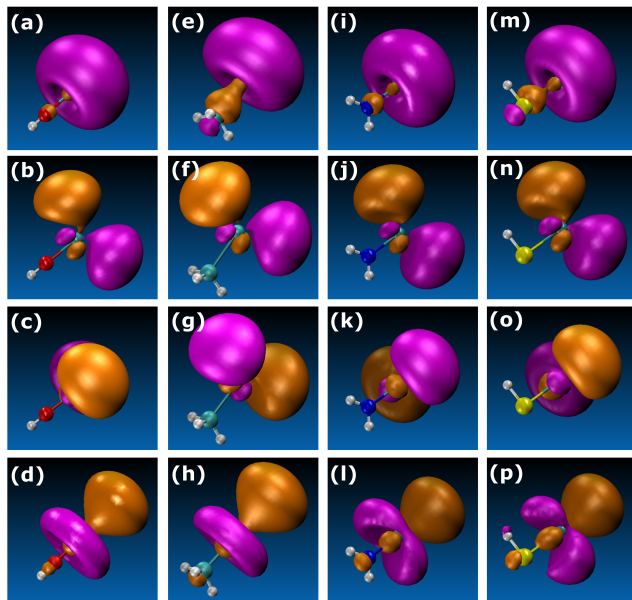


FIG. 4. Comparison of molecular orbitals for electronic transitions employed in the proposed laser cooling scheme for four ML molecules with different symmetries:  $\text{CaOH}$  (a-d),  $\text{CaCH}_3$  (e-h),  $\text{CaNH}_2$  (i-l), and  $\text{CaSH}$  (m-p). Molecular geometries are plotted for the ground electronic state; rows 1 through 4 correspond to SOMO, LUMO, LUMO+1, and LUMO+2 configurations, respectively. Molecular symmetry is incrementally reduced from column 1 to column 4:  $C_{\infty v}$ ,  $C_{3v}$ ,  $C_{2v}$ , and  $C_s$ . All isosurfaces are plotted for the isovalue of 0.03 with magenta (orange) representing positive (negative) values.

parison of the singly occupied molecular orbital (SOMO) and the lowest unoccupied molecular orbital (LUMO) as the symmetry of the ML molecule is reduced (column 1  $\rightarrow$  4). Despite significant differences in structural symmetry, for the SOMO, LUMO and LUMO+1 (rows 1-3) the molecular orbitals are essentially unchanged as the molecule distorts. The orbitals are only slightly distorted for LUMO+2 (row 4). Quantitatively, both ionic bonding and heavy valence electron localization on the metal atom are described by the Mulliken charge and spin population analyses. As the ligand is changed from OH ( $C_{\infty v}$ ) to  $\text{CH}_3$  ( $C_{3v}$ ) to  $\text{NH}_2$  ( $C_{2v}$ ) and SH ( $C_s$ ), the Mulliken charge on the Ca atom goes from +0.58 to +0.58 to +0.55 and +0.51 while the spin population changes from 0.999 to 0.908 to 0.982 and 0.963, respectively. This is in qualitative agreement with the electron affinities determined for these anion ligands [71]. The similar electronic structure in these molecules suggests that laser cooling of ATMs will proceed similarly to cooling linear species.

Losses due to purely electronic transitions are not expected to affect photon cycling in these molecules. One potential loss channel involves any electronic state intermediate to the ground and excited states used for optical cycling. Radiative decay through these intermediate states will result in a change of parity and populate dark

rovibrational states in  $\tilde{X}$  [22]. For the molecules considered here, no electronic states between the  $\tilde{A}$  and  $\tilde{X}$  states have been observed. When optical cycling with the excited  $\tilde{B}$  or  $\tilde{C}$  states, one may still worry about radiative cascades through the lower-lying  $\tilde{A}$  state. Due to the small energy spacing between the three lowest excited states ( $100\text{--}1000\text{ cm}^{-1}$ ), radiative decay rates from  $\tilde{B}$  or  $\tilde{C}$  to  $\tilde{A}$  will be suppressed by a factor of  $(\Delta\omega/\omega)^{-3} \sim 10^4$  relative to decays directly to  $\tilde{X}$ . Thus, loss due to potential two-photon cascades will come in at the same level as that observed already in experiments cooling diatomic species [18], which does not present any challenges to cooling and trapping experiments.

A second potential source of loss involves higher-order multipole transitions, e.g. M1 and E2 transitions, that would remove molecules from the optical cycle by populating opposite parity rovibrational states. M1 transitions cannot change the electronic configuration and are therefore  $\sim \omega_{M1}^3 \alpha^2 / \omega_{E1}^3 \sim 10^{-9}$  smaller than E1 transition rates, where  $\alpha \approx 1/137$  is the fine-structure constant [72]. The rate of E2 transitions is expected to be  $\sim (\omega/c)^2 \langle f|r^2|i\rangle / \langle f|r|i\rangle \sim 10^{-7}$  that of E1 transitions, where  $|i\rangle$  and  $|f\rangle$  are the initial and final states, respectively. Therefore, loss due to M1 or E2 transitions should be negligible until  $\gg 10^6$  photons have been scattered. Such effects have not yet limited diatomic laser cooling experiments, and are unlikely to affect laser cooling of ATMs [27, 32].

## B. Vibrational Branching

Accurate values of the vibrational branching ratios during an electronic decay are of utmost importance to molecular laser cooling. To date, very few measurements of vibrational branching ratios for ATMs have been performed. To provide information relevant to laser cooling, these measurements would ideally use cw excitation to a low- $J$  rotational state, be free from state-changing collisions, and include careful calibration of detection efficiency over a wide range of wavelengths. These restrictions limit the number of useful direct FCF measurements in the literature. In contrast (and fortunately), high-quality spectroscopic data (including bond lengths and angles) for many molecules of interest is plentiful. As such, we use a semi-empirical method to compute FCFs for a large set of ATMs expected to be favorable for laser cooling. When accurate high-resolution spectroscopic measurements are available, the computational methods described below can provide vibrational branching ratios in excellent agreement with observations, and with accuracy better than purely *ab initio* predictions [73, 74]. The accuracy of these calculations depends entirely on the accuracy of the measured molecular geometries. In the absence of such experimental data, *ab initio* calculations have enabled unique insights into identification of favorable ligands for laser cooling [31] and estimation of the vibrational branching ratios [75],

Franck-Condon factors, which characterize the probability of vibrational state changes in an electronic decay, are computed by evaluating the overlap integral between excited and ground vibrational wavefunctions:

$$q_{v',v''} = \left| \int \psi_{v'}(\mathbf{Q}') \psi_{v''}(\mathbf{Q}'') d\mathbf{Q}'' d\mathbf{Q}' \right|^2, \quad (1)$$

where  $\mathbf{Q}''$  represent the vibrational normal modes of the ground state and  $\mathbf{Q}'$  the vibrational normal modes of the excited state. We compute these integrals within the harmonic approximation, which is justified given that anharmonic contributions are  $\omega_e x_e / \omega_e \approx 5 \times 10^{-2}$  for the AE-containing molecules considered here are [63].

We follow standard methods to calculate the FCFs [76]. In brief, we first perform a **GF**-matrix analysis of the vibrational problem [77] to determine the normal modes in each electronic manifold. Experimentally measured vibrational frequencies are used to fit the elements of the **F** matrix. We include a Duschinsky transformation between ground and excited normal coordinates, which accounts for normal mode mixing (see Fig. 5). We then follow the method of Sharp and Rosenstock [78, 79] which uses generating functions and a linear transformation between the normal coordinates of ground and excited states to define analytic expressions for the FCFs. Analytical formulas evaluating Eq. 1 are available for various combinations of vibrational excitations [78, 80]. This model allows one to predict vibrational branching ratios for all vibrational modes within the harmonic approximation. It has been validated for many linear and non-linear polyatomic species [25, 73, 74] with excellent agreement between theory and experiment. We find that the computed FCFs depend strongly on the changes in molecular geometry upon electronic excitation and more weakly on changes in vibrational frequencies. High-resolution spectroscopy confirms that the molecular geometries change minimally upon electronic excitation [46, 48, 49].

We benchmark our multidimensional FCF calculations by comparing to experimental measurements. FCFs for  $\text{SrNH}_2$  have been previously measured [48] on the  $\tilde{C}^2A_1 \rightarrow \tilde{X}^2A_1$  and  $\tilde{A}^2B_2 \rightarrow \tilde{X}^2A_1$  bands. Table I reports the calculated vibrational branching ratios for  $\text{SrNH}_2$  and their comparison to experimentally measured values; we find excellent agreement between theory and experiment. We speculate that the small discrepancies, which occur in vibrations of the ligand, arise from the fact that the spectroscopy was typically unable to fully determine the ligand geometry, so systematic errors affecting the calculations are possible. These calculations indicate that for  $\text{SrNH}_2$ , photon cycling of  $\sim 10^4$  photons should be possible with just three vibrational repumping lasers. There also exist measurements of vibrational branching ratios in  $\text{CaOC}_2\text{H}_5$  [59], predicting a decay to the Ca-O stretching mode of  $\sim 0.1$ , in good agreement

Transition	Decay to	Calculated	Measured <sup>a</sup>
$\tilde{A} \rightarrow \tilde{X}$	$0_0$	0.960	0.959
	1x Sr-N stretch	0.039	0.04
	2x Sr-N stretch	$1 \times 10^{-3}$	$\sim 1.6 \times 10^{-3}$
	1x NH <sub>2</sub> bend	$3 \times 10^{-5}$	$2 \times 10^{-5}$
	1x N-H sym. stretch	$8 \times 10^{-6}$	$4 \times 10^{-5}$
$\tilde{C} \rightarrow \tilde{X}$	$0_0$	0.976	-
	1x Sr-N stretch	0.011	0.01
	1x N-H sym. stretch	$6 \times 10^{-6}$	$8 \times 10^{-6}$
	1x NH <sub>2</sub> bend	0.010	overlapped

<sup>a</sup> From Ref. [48]

TABLE I. Comparison of measured and calculated vibrational branching ratios for SrNH<sub>2</sub>. Because decay to the NH<sub>2</sub> bending mode is overlapped in the  $\tilde{C} \rightarrow \tilde{X}$  band, we are not able to sum experimental FCFs in this case. The molecular geometry and vibrational frequencies used in the calculations are taken from Refs. [48, 50, 81].

with our calculation below.<sup>5</sup> Besides these few cases, vibrational branching ratios for nonlinear, laser-coolable species are rarely reported. Clearly, there is need for new, accurate measurements of vibrational branching ratios in AE-containing ATMs.

Calculated multidimensional FCFs for CaNH<sub>2</sub>, CaSH, and SrSH are reported in Tab. II. Although there are no published FCF measurements for these species, high-resolution studies have noted that off-diagonal decays were either unobservably small or highly suppressed, in agreement with our predictions [63]. For these molecules, our calculations indicate that 3-5 repumping lasers will be required to scatter  $> 10^4$  photons. Generally, the calculations agree very well with the simpler model used for the predictions in Tab. III. Where differences occur, these can be attributed to mixing of normal modes that was neglected in the simple model [82]. Vibrational normal modes of MSH species are shown in Fig. 5, depicting a strong mixing between the bending and M-S stretching motions; this mixing is included in our calculations. Dynamic visualizations of all vibrational normal modes for CaNH<sub>2</sub> are provided in the media Supplemental Materials. Proper accounting of the differences between ground state and excited state normal modes is included in the calculations of Tabs. I and II. Comparison of the methods also shows that while the individual FCFs may differ slightly, the sum of the dominant few FCFs is consistent.

The computations above require the complete molecular geometry and vibrational frequencies for all vibrational modes, which have not been experimentally determined for many species. Often, only the metal-ligand

	CaNH <sub>2</sub>		
	$\tilde{A} \rightarrow \tilde{X}$	$\tilde{B} \rightarrow \tilde{X}$	$\tilde{C} \rightarrow \tilde{X}$
$0_0^0$	0.963	0.993	0.979
1x Ca-N stretch	0.034	$2 \times 10^{-3}$	0.019
1x NH <sub>2</sub> bend	$2 \times 10^{-3}$	$1 \times 10^{-3}$	$8.8 \times 10^{-4}$
2x Ca-N stretch	$1.6 \times 10^{-4}$	$5 \times 10^{-5}$	$3.6 \times 10^{-6}$
1x N-H sym. stretch	$3.1 \times 10^{-7}$	$3 \times 10^{-6}$	$3.3 \times 10^{-7}$
	CaSH		
	$\tilde{A} \rightarrow \tilde{X}$	$\tilde{B} \rightarrow \tilde{X}$	$\tilde{C} \rightarrow \tilde{X}$
$0_0^0$	0.820	0.952	0.999
1x Ca-S stretch	0.163	0.0276	$3.3 \times 10^{-4}$
1x Ca-S-H bend	0.016	0.0199	$3.5 \times 10^{-6}$
2x Ca-S stretch	$1.6 \times 10^{-4}$	$4 \times 10^{-4}$	$< 10^{-6}$
1x S-H stretch	$1 \times 10^{-6}$	$1 \times 10^{-6}$	$1 \times 10^{-6}$
	SrSH		
	$\tilde{A} \rightarrow \tilde{X}$	$\tilde{B} \rightarrow \tilde{X}$	$\tilde{C} \rightarrow \tilde{X}$
$0_0^0$	0.828	0.953	0.976
1x Sr-S stretch	0.170	0.046	0.023
1x Sr-S-H bend	0.0014	$4 \times 10^{-4}$	$2 \times 10^{-4}$
2x Sr-S stretch	$1 \times 10^{-4}$	$< 10^{-5}$	$< 10^{-4}$
1x S-H stretch	$1 \times 10^{-6}$	$1 \times 10^{-6}$	$1 \times 10^{-6}$

TABLE II. Calculated multidimensional FCFs for CaNH<sub>2</sub>, CaSH, and SrSH. The molecular geometry and vibrational frequencies used in the calculations are as reported in Refs. [46, 47, 49, 54-56, 63].

bond lengths have been determined. Experience with the monohydroxides shows that the metal-ligand stretching mode is typically the dominant decay channel. Table III presents metal-ligand stretching mode FCFs for a wide variety of species [82]. The FCFs for these ATMs are highly diagonal due to the small changes in potential energy surface shapes upon decay. We estimate the relative error in our calculations by using the same model for compute FCFs for isoelectronic diatomic and linear triatomic species; for the diagonal FCFs, the relative error is expected to be  $< 3\%$ . Note that perturbations in the excited electronic state can introduce unexpectedly strong off-diagonal decays [73], and for any particular species the dominant uncertainty in the FCFs will likely be due to these perturbative couplings. These will become more prevalent especially with increasing complexity and decreasing symmetry of the ligand (see App. A).

We have also conducted a set of *ab initio* calculations to understand these species (see App. B). Normal modes and vibrational frequencies were computed at optimized geometries using the ORCA Quantum Chemistry Software [84] and wavefunction overlap integrals were computed numerically using the ezSpectrum software [85]. The calculations are benchmarked by testing the predictions for CaOH against experimentally determined FCFs [73]. For the lowest excited electronic tran-

<sup>5</sup> These measurements were taken with pulsed-laser excitation and the data shows signs of collisional excitation which could present systematic errors in their interpretation.

Molecule	Transition	$q_{00}$	$q_{01}$	$\lambda_{00}$ (nm)	$\lambda_{01}$ (nm)
CaSH	$\tilde{A} \rightarrow \tilde{X}$	0.826	0.157	650	664
	$\tilde{B} \rightarrow \tilde{X}$	0.983	0.016	630	643
	$\tilde{C} \rightarrow \tilde{X}$	0.999	0.0003	622	634
SrSH	$\tilde{A} \rightarrow \tilde{X}$	0.850	0.137	700	713
	$\tilde{B} \rightarrow \tilde{X}$	0.962	0.037	675	687
	$\tilde{C} \rightarrow \tilde{X}$	0.981	0.0184	666	678
MgNH <sub>2</sub> <sup>a</sup>	$\tilde{A} \rightarrow \tilde{X}$	0.933	0.065	$\sim 410$ <sup>b</sup>	$\sim 420$ <sup>b</sup>
CaNH <sub>2</sub>	$\tilde{A} \rightarrow \tilde{X}$	0.964	0.035	640	662
	$\tilde{B} \rightarrow \tilde{X}$	0.997	0.0002	633	654
	$\tilde{C} \rightarrow \tilde{X}$	0.976	0.022	576	593
SrNH <sub>2</sub>	$\tilde{A} \rightarrow \tilde{X}$	0.957	0.039	700	723
	$\tilde{B} \rightarrow \tilde{X}$	0.971	0.028	679	700
	$\tilde{C} \rightarrow \tilde{X}$	0.956	0.013	630	648
BaNH <sub>2</sub> <sup>c</sup>	$\tilde{A} \rightarrow \tilde{X}$	0.916	0.081	$\sim 895$ <sup>b</sup>	$\sim 925$ <sup>b</sup>
	$\tilde{C} \rightarrow \tilde{X}$	0.851	0.137	$\sim 760$ <sup>b</sup>	$\sim 780$ <sup>b</sup>
MgCHDT	$\tilde{A} \rightarrow \tilde{X}$	0.936	0.062	499	526
CaCHDT	$\tilde{A} \rightarrow \tilde{X}$	0.997	0.002	680	700
CaOCHDT	$\tilde{A} \rightarrow \tilde{X}$	0.951	0.048	628	648
	$\tilde{B} \rightarrow \tilde{X}$	0.946	0.046	565	586
SrOCHDT	$\tilde{A} \rightarrow \tilde{X}$	0.945	0.046	689	709
CaSCH <sub>3</sub>	$\tilde{A} \rightarrow \tilde{X}$	0.809	0.171	645	658
	$\tilde{B} \rightarrow \tilde{X}$	0.981	0.018	633	645
SrSCH <sub>3</sub>	$\tilde{A} \rightarrow \tilde{X}$	0.832	0.153	694	706
	$\tilde{B} \rightarrow \tilde{X}$	0.978	0.021	676	688
	$\tilde{C} \rightarrow \tilde{X}$	0.957	0.042	647	657
CaNHCH <sub>3</sub>	$\tilde{A} \rightarrow \tilde{X}$	0.953	0.046	652	673
SrNHCH <sub>3</sub>	$\tilde{A} \rightarrow \tilde{X}$	0.944	0.054	706	726
CaOC <sub>2</sub> H <sub>5</sub>	$\tilde{A} \rightarrow \tilde{X}$	0.892	0.102	631	647
CaOCH(CH <sub>3</sub> ) <sub>2</sub>	$\tilde{A} \rightarrow \tilde{X}$	0.956	0.043	632	645
SrOCH(CH <sub>3</sub> ) <sub>2</sub>	$\tilde{A} \rightarrow \tilde{X}$	0.943	0.056	690	704
CaC <sub>5</sub> H <sub>4</sub> CH <sub>3</sub> <sup>d</sup>	$\tilde{A} \rightarrow \tilde{X}$	0.825	0.094	691	706
	$\tilde{B} \rightarrow \tilde{X}$	0.86	0.078	686	701

<sup>a</sup> Mg-N bond lengths inferred from Refs. [51, 52, 83].

<sup>b</sup> Excitation wavelengths not measured at high resolution.

<sup>c</sup> Ba-N bond lengths inferred from Refs. [31, 53].

<sup>d</sup> Dispersed fluorescence measured in Ref. [61].

TABLE III. Franck-Condon factors calculated for decay to 0 quanta ( $q_{00}$ ) and 1 quantum ( $q_{01}$ ) of the metal-ligand stretching mode.  $\lambda_{00}$  and  $\lambda_{01}$  are the main cycling and first repumping transition wavelengths in nm. Experimentally measured geometries and frequencies come from Refs. [46–64, 67, 68].

sition  $\tilde{A} \rightarrow \tilde{X}$ , the FCF for the fundamental  $0_0^0$  transition changed from 0.988 (CaOH) to 0.870 (CaSH) to 0.989 (CaNH<sub>2</sub>). The dominant vibrational loss channel was to the Ca-ligand stretching mode for all three molecules with decay fractions 0.01 (CaOH), 0.10 (CaSH) and 0.01 (CaNH<sub>2</sub>) to this mode. The Duschinsky transformation [86] of the normal modes was used for all three

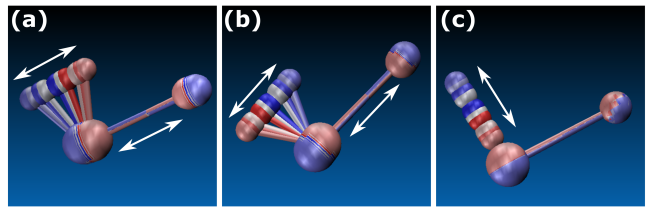


FIG. 5. Normal modes for CaSH corresponding to (a) 316  $\text{cm}^{-1}$ , (b) 360  $\text{cm}^{-1}$  and (c) 2640  $\text{cm}^{-1}$  vibrational frequencies. The beginning of the trajectory is indicated in red, the middle in white, and the end in blue. Note the strong mixing between the bending motion and Ca-S stretching vibration.

molecules to account for the change in normal coordinates in each electronic state. In the case of CaSH, we observed strong mixing between the stretching and bending motions (see Fig. 5). While the CaSH  $0_0^0$  vibronic FCF is predicted to be  $< 0.9$ , the sum of the three dominant vibrational loss channels is  $\gtrsim 0.99$ . Previous work [75] has indicated that only the sum of the three dominant FCFs should be considered stable for predictive purposes when purely *ab initio* methods are being used.

Based on these calculations and their agreement with experiment, ATMs are strong candidates for optical cycling and laser cooling. For species of the form MSH and MNH<sub>2</sub> (M=Mg, Ca, Sr), the calculations indicate that at least one electronic transition in several of the species considered can scatter  $> 10^3$  photons with only a single repumping laser. The calculations predict that the number of photon scatters per molecule is increased to  $> 10^4$  per molecule—the typical number required to slow a molecular beam and capture into a MOT—with three repumping lasers. Indeed, the calculated FCFs are comparable to those of isoelectronic diatomic species which have already been successfully laser-cooled [17, 18]. For the larger species, at least 100 photons can be scattered with just two lasers. It is remarkable that even in species as complex as calcium methycyclopentadienyl [CaC<sub>5</sub>H<sub>4</sub>CH<sub>3</sub>, Fig. 2(g)], with 36 vibrational normal modes, the FCFs converge to  $\gtrsim 0.95$  with just one or two repumping lasers [61]. This is sufficient for high-fidelity detection, preparation of single quantum states, or transverse laser cooling in order to enhance interrogation times in a molecular beam [24, 44] (see Sec. III B).

### C. Rotational Branching

Laser cooling requires, in addition a vibrationally closed optical cycle, rotationally closed transitions. The rotational structure of ATMs can be extremely complex (see App. C). Following standard convention, we label the rotational states by  $N_{K_a K_c}$ .  $N$  is the total angular momentum excluding electron and nuclear spins. The principal rotational constants are labeled  $A$ ,  $B$ , and  $C$ , where  $A > B > C$ .  $K_a$  and  $K_c$  are not rigorous quan-

tum numbers, but are defined as the projection of  $N$  onto the hypothetical symmetry axis formed by distorting the molecule to prolate ( $a$ -axis) and oblate limits ( $c$ -axis), respectively. Note that a Hund's case (b) basis is often most convenient as  $N$  is an approximately good quantum number. Due to the unpaired electron spin, which can couple weakly to rotation,  $J = N + S$  is the total angular momentum excluding nuclear spin. Hyperfine structure is typically unresolved ( $< 1$  MHz). Losses to dark states throughout the complicated rotational ladder are a potential concern during photon cycling. Here we show that rotational and parity selection rules can eliminate or mitigate these potential problems.

In a generic ATM, the transition dipole moment,  $\hat{\mu}$ , can have components along any of the three principal axes. The transition dipole moment components are labeled  $\hat{\mu}_a$ ,  $\hat{\mu}_b$ , and  $\hat{\mu}_c$  to indicate their projection along the principal axes of the molecule. The transitions are then labeled  $a$ -type,  $b$ -type, or  $c$ -type according to which component of the transition dipole moment they couple. For a molecule nearer the prolate limit,  $b$ - and  $c$ -type transitions are “perpendicular” while  $a$ -type transitions are “parallel.” The selection rules for each type of transition are summarized in Tab. IV. There are additional restrictions due to the fact that  $K_a + K_c = N$  or  $N + 1$  [87, 88]. The selection rules and their symmetry considerations are discussed in detail in App. D.

Using the selection rules enumerated in Tab. IV we find that it is possible to construct closed cycling schemes for transitions coupling to any component of  $\hat{\mu}$ . Some representative photon cycling schemes are presented in Fig. 6. Dashed lines indicate rotational branches which may be induced by spin-rotation mixings in some cases (see App. D for intensity estimates). In well-behaved cases, the dashed lines may not require repumping. An  $a$ -type band, expected for the  $\tilde{C} \leftarrow \tilde{X}$  transitions, is shown in Fig. 6(a). The rotational structure is reminiscent of a  $(b)^2\Sigma^+ \leftarrow (b)^2\Sigma^+$  transition in linear molecules, where the first letter indicates the appropriate Hund's case.<sup>6</sup> In this case, a combination of parity and angular momentum selection rules guarantee rotational closure when driving

	$\Delta K_a$	$\Delta K_c$	Exceptions
$a$ -type	0	$\pm 1$	$\Delta N \neq 0$ for $K'_a \rightarrow K''_a = 0$
$b$ -type	$\pm 1$	$\pm 1$	
$c$ -type	$\pm 1$	0	$\Delta N \neq 0$ for $K'_c \rightarrow K''_c = 0$

TABLE IV. Selection rules in the dipole approximation for transitions proposed ATM laser-cooling transitions. Higher order decays ( $\Delta K_c = \pm 2$ , etc.) are suppressed, but may be induced by perturbations. There is an additional restriction due to the fact that  $K_a + K_c = N$  or  $N + 1$  [87, 88].

<sup>6</sup> Such a transition is used for laser slowing of CaF molecules [18] and laser cooling of SrOH molecules [24].

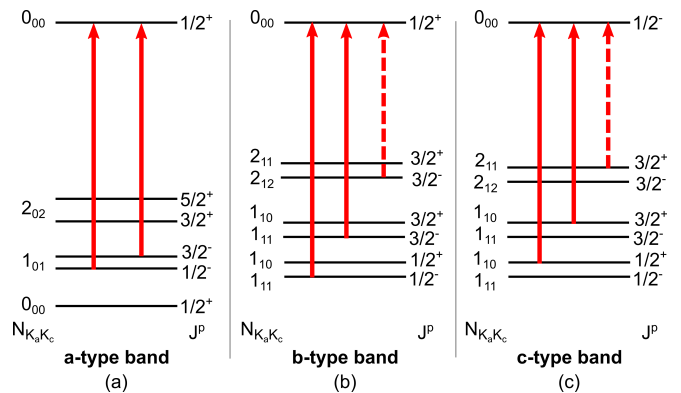


FIG. 6. Schemes to achieve rotationally-closed photon cycling for pure (a)  $a$ -type transitions, (b)  $b$ -type transitions, and (c)  $c$ -type transitions. Dashed lines indicate transitions which will need to be repumped in special cases, as described in the text. In the  $K_a = 1$  levels, the spin-rotation and asymmetry doubling are approximately the same size. These level diagrams assume a near-prolate ATM, but analogous results apply for near-oblate tops.

the  ${}^Q Q_{12}(0, 1, 0.5)$  and  ${}^Q P_{11}(0, 1, 1.5)$  lines.<sup>7</sup> A single rf sideband, easily generated using an electro-optic modulator (EOM) or acousto-optic modulator (AOM), must be added to the excitation laser. Figure 6(b) shows a scheme for rotational closure on a  $b$ -type band, typical of  $\tilde{A} \leftarrow \tilde{X}$  transitions. Here, excitation out of the  $K''_a = 1$  sublevel is convenient because it allows one to target the lowest level of the excited electronic state. In this case, we drive the  ${}^P Q_{12}(1, 1, 0.5)$  and  ${}^P P_{11}(1, 1, 1.5)$  lines. Figure 6(c) shows how to achieve rotational closure on a  $c$ -type band, applicable to the  $\tilde{B} \leftarrow \tilde{X}$  transitions. The  $b$ - and  $c$ -type bands shown here are similar to a  $(b)^2\Sigma^\pm \leftarrow (b)^2\Pi$  transition in linear species.<sup>8</sup> Here, we choose to drive the  ${}^P Q_{12}(1, 0, 0.5)$  and  ${}^P P_{11}(1, 0, 1.5)$  lines. Similar to the  $a$ -type band, an rf sideband is required to address the two spin-rotation components of the  $N'' = 1$  manifold for either  $b$ -type or  $c$ -type bands. Note that the  $K''_a = 1$  state, which is convenient for optical cycling, provides a suitable ground state because it is metastable with lifetimes  $\gg 10$  s for the species considered here.

The cycling schemes in Fig. 6 provide a basis for rotational closure in realistic molecules. Roughly speaking,  $\tilde{A} \rightarrow \tilde{X}$  decays follow  $b$ -type selection rules,  $\tilde{B} \rightarrow \tilde{X}$  decays obey  $c$ -type selection rules, and  $\tilde{C} \rightarrow \tilde{X}$  decays obey  $a$ -type selection rules. As the molecule becomes more asymmetric these patterns will break down and a given excited state may decay via one of several components of  $\hat{\mu}$ . A hybrid  $ab$ -type band will commonly occur for molecules with  $C_s$  symmetry due to the misalignment of the principal axes from the electronic orbitals [see

<sup>7</sup> We use the branch designation  $\Delta K_a \Delta J_{F'_n F''_n}(K''_a, K''_c, J'')$ , where  $F_n$  labels the spin-rotation component.

<sup>8</sup> Such a transition is proposed for laser cooling the CH radical [89].

Fig. 4(m-p)]. One additional decay must be repumped, in essence combining the schemes in Fig. 6(a) and (b). Alternatively, microwave remixing within the ground manifold can return population to the optical cycle. The degree of asymmetry will determine the relative strengths of different components of  $\hat{\mu}$ . For example, because  $\hat{\mu}_a \gg \hat{\mu}_c$  when photon cycling on the  $\tilde{C} \leftarrow \tilde{X}$  band of hydrosulfide species, these can scatter  $\sim 10^4$  photons using the scheme of Fig. 6(a) before repumping of the  $K_a'' = 1$  state is required (see Apps. B and D). For hybrid  $bc$ -type decays, which may occur in molecules with symmetry lower than  $C_s$  or due to perturbations, repumping is easily achieved by combining the schemes of Fig. 6(b) and (c). A single laser with sidebands imposed by EOMs or AOMs can bridge the full spin-rotation/asymmetry doubling structure. Finally, for species with near- $C_{3v}$  symmetry (e.g. MOCHDT or MCHDT), where the  $\tilde{A}^2A'$  and  $\tilde{B}^2A''$  states have essentially coalesced into the  $\tilde{A}^2E$  level, an additional decay to the  $2_{1K_c}(J'' = 3/2)$  state will appear. Again, this state can be remixed using either microwaves or a single additional laser frequency, as shown by dashed lines in Fig. 6. The effects of perturbations, though not expected to significantly alter the results presented above, are discussed in App. D. Overall we see that, despite the complex ATM rotational structure, application of one or two lasers (depending on the molecular species) with appropriate rf sidebands leads to rotational closure sufficient for scattering  $\gtrsim 10^6$  photons. Remarkably, this level of complexity is comparable to that required for laser cooling of diatomic species for which rotational repumping is implemented [17, 22, 41, 90].

#### D. General Principles

The detailed calculations of the previous section focused on select species that have been observed in prior experiments. These calculations elucidate many general principles which apply to the whole class of ATMs with optical cycling centers.

First, the key features of the electronic structure in the species discussed here derive from the metal-centered valence electron, with potential energy surfaces which vary little from one electronic state to another. Our calculations show that the ligand’s asymmetry does not strongly perturb the electronic distribution; the electronic distribution is similar to that expected from a simple diatomic model, independent of the structural asymmetry of the ligand. This crucial feature leads to the possibility of photon cycling. Molecules containing other AE or AE-like atoms, e.g. Be, Mg, Ba, or Yb, should have analogous electronic structure and be favorable for laser cooling. Certain of these AE (or AE-like) atoms may be ideal for particular applications (see Sec. IV). For instance, the low mass of Be could be beneficial to studies involving torsional modes, while the high- $Z$  Yb nucleus can enhance symmetry violating effects. The relative insensitivity of the electronic structure to the AE atom’s

identity means that the ideas presented above apply to a very wide range of species, aiding the task of searching for promising candidates. Beyond molecules with AE atoms, several laser-coolable molecules have been identified containing cycling centers from group 3 or 13 of the periodic table, notably TiO [33], AlF [91], TlF [92], and BH [93]. We expect that ATM species isoelectronic to these (AlSH, TlOCH<sub>2</sub>CH<sub>3</sub>, etc.) will also have highly diagonal FCFs. However, to date such species have received little or no spectroscopic attention.

Second, although the FCFs do not follow selection rules present for linear species, we have shown that they are still highly constrained and amenable to photon cycling/laser cooling. In general, the off-diagonal decay strengths do not increase as the molecule becomes “more” asymmetric. Rather, the strengths remain weak so long as the potential energy surfaces are similar in ground and excited state. Based on the geometry changes measured by high-resolution spectroscopy and predicted by our *ab initio* calculations, this is the case for the broad class of molecules explored here. As expected, it is the *change* in geometry which drives the FCFs, rather than the geometry itself [76, 78]. While a dedicated vibrational analysis will be required for any particular molecule, our calculations indicate that dozens of ATM species are highly amenable to photon cycling. While vibrational anharmonicity is small for the molecules considered here, its presence may be an important consideration if “floppier” ATMs are of interest in the future. This will particularly be the case for species which include relatively long carbon chains.

Third, we have seen how the leakages due to rotational branching can be mitigated or wholly eliminated by working with low- $J$  states and approximate rotational selection rules. While we considered primarily the near-prolate limit, molecules near the oblate limit behave analogously but with  $K_a$  and  $K_c$  interchanged. Even for chiral molecules near the prolate (or oblate) limit, the same rotational closure schemes are expected to be applicable. The strength of hybrid rotational branches is expected to increase with the degree of structural asymmetry. Additionally, off-diagonal terms in the rotational Hamiltonian (see App. C) may admix levels with  $\Delta K_a = \pm 2$  and  $\Delta K_c = \pm 2$  selection rules. However, these matrix elements conserve  $J$  so that for the low- $J$  states considered here the Hamiltonian is still highly restricted. Transitions with  $\Delta K_a = \pm 2, \pm 3, \dots$  (and similarly for  $\Delta K_c$ ) are limited by the restriction that  $K_a + K_c = N$  or  $N+1$ . In the absence of strong perturbations, even highly asymmetric species will likely require at most one or two additional laser or microwave frequencies to achieve rotational closure. The rotational level structure for any given molecule will be determined by the particular values of  $A$ ,  $B$ , and  $C$ , and the levels will not necessarily group into nearly-spaced sets of levels labeled by  $K_a$  (prolate) or  $K_c$  (oblate). As shown above, in the absence of strong perturbations our proposed rotational pumping schemes require an additional frequency (either mi-

crowave or optical) per vibrational band.

### III. EXPERIMENTAL OUTLOOK

#### A. Molecule production

The molecules considered above can be generated in a straightforward manner using the cryogenic buffer-gas cooling method, which has been used in all molecular laser cooling experiments to date [27, 32, 94]. Ablation of a metallic target into a reactant gas, followed by buffer-gas cooling due to collisions with cryogenic He can be used, as has been demonstrated with  $\text{Ca} + \text{SF}_6$  [18] and  $\text{Yb} + \text{CH}_3\text{OH}$  [25]. Commercially available reactants such as hydrogen sulfide, ammonia, chiral methyl fluoride, thiols, pentadienyls, etc. can be introduced with a heated capillary to produce the species considered above. Typical yields of  $\sim 10^{10}$  molecules per ablation pulse have been demonstrated for a variety of molecules [94]. Production can be enhanced by an order of magnitude by exciting the ablated metal atoms to the metastable  $^3P_1$  state [63, 64, 95]. Especially for larger molecules, buffer-gas cooling provides invaluable phase-space compression and limits the number of populated vibrational modes such that significant molecular population is available for manipulation.

This internal cooling enhances the population in low-lying rotational states by several orders of magnitude without significantly boosting the forward velocity of a beam extracted from the cryogenic cell. Rotational cooling is an important consideration when deciding on the exact photon cycling scheme to employ. For species without reflection symmetry, population will be cooled into the lowest  $K_a'' = 0$  state, with a smaller amount of population in  $K_a'' = 1$ . On the other hand, molecules with  $C_{2v}$  symmetry (e.g.,  $\text{MNH}_2$ ) will cool into both the  $K_a'' = 0$  or  $K_a'' = 1$  levels due to nuclear spin statistics as previously observed in supersonic beams [50]. Because populating the  $K_a'' = 1$  level is often useful for photon cycling, we emphasize that it is straightforward to populate this level for any of the species discussed here using microwaves, optical pumping, or natural population.

#### B. From Photon Cycling to Laser Cooling

For the molecules considered in Tab. III (and assuming a reasonable number of lasers), the number of photons that can be scattered before loss to a dark state can vary considerably. It is therefore worthwhile to enumerate the advantages of optical cycling over a range of different “photon budgets.”

First, consider the case where vibrational leakage channels are closed at the  $10^{-2}$  level; this allows  $\sim 10 - 100$  photon scatters per molecule before significant loss to a vibrational dark state. This level of photon scattering

allows quantum state preparation and high-fidelity read-out, allowing 100% detection fidelity for each molecule in a beam [96, 97]. Well-developed optical pumping and coherent population transfer techniques [98] would be enabled, a significant advantage to molecular beam experiments described below. Given the FCFs calculated above, each of the molecules considered in Tab. III would fall in this regime given an experiment using a single vibrational repumping laser.

If vibrational losses are controlled at the  $10^{-3}$  level,  $\sim 1,000$  photons may be scattered by each molecule before significant loss to a dark state. Such a photon budget is sufficient for transverse laser cooling of linear molecules, decreasing molecular beam divergence and increasing phase-space density by at least an order of magnitude [24, 25, 44]. Feasible coherence times for measurements using transversely cooled molecules would increase by factors of  $10 - 100$ . In addition, this level of photon scattering would make possible slowing of a molecular beam to the capture velocity of a molecular MOT using novel techniques like the coherent bichromatic force or pulsed laser deceleration [99–101] or a Zeeman-Sisyphus decelerator [102]. For the molecules proposed in Tab. III, scattering  $\sim 10^3$  photons will likely require 3-5 lasers, strongly dependent on the particular molecule.

A “full” laser cooling experiment can be modeled after recent work in diatomic species [27, 32]. Given typical molecular masses ( $\sim 50 - 100$  amu) and buffer-gas beam source velocities ( $\sim 70 - 100$  m/s), roughly 20,000 photon scatters are required to slow a molecule to rest. Furthermore, at typical scattering rates of  $\sim 10^6$  s $^{-1}$ , another 5,000 – 10,000 photons are required for capture into a magneto-optical trap and cooling to the Doppler limit. Modeling loss to vibrational dark states as a Poisson process, in order to scatter  $\sim 30,000$  photons without losing more than about half of the molecular population requires repumping all decays that appear at the  $> 5 \times 10^{-5}$  level. Such a level of photon scattering would enable the full range of techniques developed in the atomic physics community: optical trapping, transfer to optical tweezers, and full quantum control of individual molecules. Based on the calculations described above, this level of closure is expected to require between 5 and 7 vibrational repumpers. Ref. [103] showed that the forces, and therefore capture velocity, of a typical magneto-optical trap (MOT) grow with increasing excited state  $g$ -factor; small excited  $g$ -factors in the  $\tilde{A}^2\Pi$  state have been a common problem for molecular MOTs. Excited state  $g$ -factors of the ATMs discussed here may be large ( $\sim 1$ ) due to the quenched orbital angular momentum. This would increase the MOT capture velocity and forces, easing the loading and cooling processes.

### IV. APPLICATIONS

Many exciting avenues will be enabled by photon cycling and laser cooling of ATMs. Applications span a

broad array of fields, accessing the full breadth of modern physics and chemistry research. In what follows we highlight many promising research directions. It is our hope that this work inspires further exploration of the applications of photon cycling and laser cooling applied to ATMs.

## A. Quantum Computation and Simulation

### 1. Information Storage

Ultracold molecules with large electric dipole moments are an exciting new platform for quantum simulation and information processing [104–108]. Recently, Albert, Covey and Preskill [109] have proposed to use 3D rigid rotor molecular codes (i.e. coherent superpositions of several molecular orientations of ATMs) to construct robust encoding of quantum information that is protected against both momentum kicks and orientation diffusion. The structural asymmetry of these three-dimensional rigid rotors, whose orientation is described as an element of the 3-dimensional rotation group  $SO(3)$ , is exactly what allows for robust encoding of information in the manifold of rotational quantum states. Such quantum error-correcting codes for ATMs like CaSH may enable robust storage and coherent processing of quantum information in a scalable experimentally-accessible manner within the near future.

The rich internal structure of dipolar molecules also allows the implementation of qudits, higher dimensional analogs of two-level qubits [110]. Compared to qubits, qudits can be more robust [111, 112] and offer improved error correction [113, 114]. The number of  $d$ -level qudits required to produce a Hilbert space of a given size is a factor of  $\log_2 d$  smaller than the number of qubits required. Similarly, the computational time to carry out a given set of gate operations using transformations in the  $d$ -dimensional space is reduced by a factor of  $(\log_2 d)^2$  [110]. As discussed in Ref. [110], the rotational and hyperfine levels in dipolar molecules can be used to form a qudit; the authors showed how to construct four-level qudits using diatomic molecules with  $^1\Sigma$  and  $^2\Sigma$  ground states. The rotational levels in ATMs can be used similarly, although with a much larger number of states available. Importantly, not only are there *more* low-lying (metastable) rotational states to manipulate, but many more of these levels are coupled to one another by dipole allowed transitions [115].

### 2. Molecule-Molecule Coupling

In addition to quantum information storage, ultracold ATMs are a promising platform for quantum information *processing* due to their strong dipole-dipole interactions. In such experiments, the interaction between two neighboring molecules scales like  $d^2$ , so choosing species with

the largest possible dipole moment is of utmost important. To date, the laser-coolable species proposed for these applications have relatively small dipole moments  $\sim 1 - 2$  D. The diatomic species cooled so far cannot be fully polarized with reasonable laboratory fields, so microwave mixing may be employed which further reduces the achievable dipole moments. Bent ATMs generically have large dipole moments due to the increasingly covalent metal-ligand bond. In addition, they can have multiple dipole moment components, one along each principal axis. For example, CaSH has a large dipole moment of  $\sim 5.5$  D along the  $a$ -axis and an additional dipole moment of  $\sim 1.5$  D along the  $b$ -axis [29].<sup>9</sup> For the same interparticle spacing, ATMs therefore offer a viable route to achieving molecule-molecule couplings at least an order of magnitude stronger than can be achieved with diatomic species laser cooled to date [32]. Figure 7 shows the lab-frame dipole moments of CaSH in several rotational states; note that the molecule is fully polarized at applied fields  $\lesssim 100$  V/cm.

As a simple example, consider two fully polarized CaSH molecules in optical tweezers separated by  $\sim 1$   $\mu\text{m}$ . In this case, achievable dipole-dipole interaction rates are  $\sim 900$  Hz (2 kHz) in the  $1_{10}/1_{11}$  ( $2_{20}/2_{21}$ ) manifold. An illustrative comparison can be made against CaF, for which rates  $\sim 100$  Hz are expected due to the smaller body-frame dipole moments and the greater difficulty to polarize. For any given separation, we expect the dipolar exchange rates of fully polarized ATMs to exceed their (fully polarized) monofluoride counterpart by about 1-2 orders of magnitude. At the small electric fields shown in Fig. 7, CaSH will be fully polarized while CaF will not be; in this more realistic case, the interaction between two ATMs will exceed that between two CaF molecules by about 3 orders of magnitude.

Use of oriented molecules has been of great interest in recent years [117–119]. ATMs with an unpaired electron spin extend these proposals yet further. We propose a simple scheme to polarize the molecule in order to access both of these dipole moments. A DC electric field  $\sim 400$  V/cm is used to mix the opposite parity  $1_{10}$  and  $1_{11}$  states and induce a dipole moment along the  $a$ -axis. Figure 7 shows the Stark structure typical for an MSH molecule in a DC electric field, using the molecular constants of CaSH. The spectrum is essentially identical to that of symmetric tops already proposed for quantum information schemes [108]. At the same time, a microwave field is used to mix the Stark-shifted state with one of the  $1_{01}$  states. This induces an orientation along the  $b$  axis. In this way, the molecule may be aligned along one axis and oriented along an axis perpendicular to it.

Following the very fruitful theoretical work on using diatomic molecules with both electric and magnetic dipole

<sup>9</sup> The bent structure is an important contributor to this larger  $a$ -axis dipole moment as can be seen by comparing the cases of CaSH ( $d \approx 5.5$  D) and CaOH ( $d \approx 1.4$  D) [29, 116].

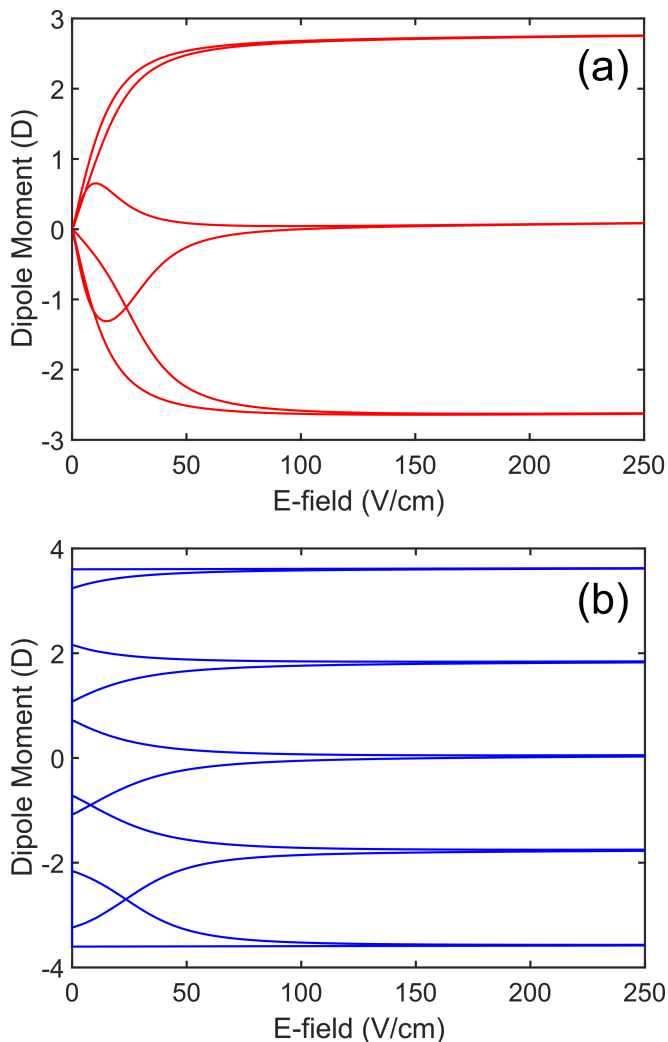


FIG. 7. Ground state dipole moments of CaSH as a function of electric field. (a) Dipole moments in the  $1_{10}/1_{11}$  asymmetry doublet. (b) Dipole moments in the  $2_{20}/2_{21}$  asymmetry doublet. Full alignment is achieved at fields  $\lesssim 100$  V/cm for  $1_{1K_c}$  and  $\ll 100$  V/cm for  $2_{2K_c}$ . Note that, even at the maximum fields shown in these plots (250 V/cm), the diatomic species CaF would only achieve a lab-frame dipole moment of 10-100 $\times$  smaller.

moments for quantum simulation protocols, our hope is that the experimental platform presented here will inspire theoretical inquiry into the use of ATMs with multiple large electric dipole moments.

### B. Time-Variation of Fundamental Constants

Variations of fundamental constants such as the proton-to-electron mass ratio,  $\mu = m_p/m_e \sim 1836$ , are predicted in many models that extend the Standard Model of particle physics [120]. Large-amplitude motions in polyatomic species, such as inversion and hindered rotation, have been predicted to yield orders-of-magnitude

enhanced sensitivity to  $\mu$  variation [121]. These motions are present in any molecule containing an internal rotor with local  $C_{3v}$  symmetry, but have no analog in linear or symmetric top molecules. For instance, torsion-rotation transitions in both methanol ( $\text{HOCH}_3$ ) and methyl mercaptan ( $\text{HSCH}_3$ ) have been found to offer significant enhancement factors [122–124]. Table III includes the laser-coolable analogs of these molecules, e.g.  $\text{CaSCH}_3$ . If lower mass is desired, Be or Mg atoms could be substituted in place of Ca. Similarly,  $\text{CaOC}_2\text{H}_5$ ,  $\text{CaC}_5\text{H}_4\text{CH}_3$ , and  $\text{CaNHCH}_3$  offer methyl groups with hindered internal rotations that may offer large enhancement factors for tests of  $\mu$ -variation. Efficient state preparation, unit-efficiency readout, phase-space compression for enhanced counting statistics, and long interrogation times enabled by laser cooling may make these systems ideal testbeds.

### C. Chiral Species

The single chirality of many biological molecules (left-handed amino acids but right-handed sugars) has fascinated physicists, chemists, and biologists for over a century. The origin of this biomolecular homochirality remains largely unsolved despite its vital implications for our understanding of the formation and evolution of life on Earth [7, 8]. Precision spectroscopy of cold chiral molecules, searching for the slight energy difference between enantiomers, could elucidate some aspects of this fundamental symmetry violation. The long interrogation times enabled by traps could greatly enhance the precision of this spectroscopy, but producing trapped samples of chiral methyl derivatives is difficult due to the small electromagnetic moment of these molecules. Direct laser cooling of chiral molecules may represent a viable alternative, one in which photon cycling and laser cooling of an ATM is unavoidable. The crucial advantage of this method is that the laser cooling properties are determined primarily by the metal atom. Because the parity-violating energy difference scales strongly with nuclear charge, the heavy radicals  $\text{BaOCHDT}$  or  $\text{YbOCHDT}$  can be considered without sacrificing good laser cooling properties. Even in the absence of laser cooling to ultralow temperatures, photon cycling of  $\sim 100$  photons would allow high fidelity quantum state preparation and readout [97].

### D. Chalcogens, Thiols, and Hydrocarbons

Recent work has demonstrated unprecedented control of molecular dissociation, including controlled dissociation in which no additional kinetic energy is imparted to the molecular fragments [125]. Such techniques have been proposed as a promising route to produce a variety of ultracold *atoms* [126, 127] and can be used to produce molecular fragments such as SH,  $\text{SCH}_3$ , S,  $\text{NH}_2$ ,

$C_4H_4CH_3$ , or  $OC_2H_5$  with even lower kinetic energy distributions to their (laser-coolable) parent molecules.

The chalcogens (S, Se, or Te) display fascinating chemistry which differs dramatically from that of the isoelectronic O atom. This is due to the fact that chalcogens have vacant  $d$ -orbitals, plus lower electronegativity and higher polarizability as compared to O. The thiols and heavy chalcogens proposed in this work represent an expansion of the chemical diversity of laser-cooled polyatomic species. Thiols and sulfides form self-assembled monolayers far more actively than other functional groups [128]. Recent spectroscopic work has attempted to understand the metal-sulfur bonding by studying the simplest diatomic analog, the AuS molecule [129], and lower temperatures may enable more detailed understanding.

At ultralow temperatures, where targeted chemistry at the bond-specific level is conceivable, one may be able to unravel subtleties of the sulfur-metal bond as compared to its oxygen-metal counterpart. The production methods described in Sec. III A can be readily adapted to produce more exotic chalcogen-containing polyatomic molecules, for example by ablating AE-metals in the presence of selenic acid ( $H_2SeO_4$ ) or telluric acid ( $Te(OH)_6$ ).

Metal atoms bound to unsaturated carbon rings have long been of interest to chemistry, dating back to the discovery of the structure of the “sandwich” molecule ferrocene,  $Fe(C_5H_5)_2$  [36]. This led to interest in producing “half-sandwich” gas-phase molecules like MCp, with Cp =  $C_5H_5$  the cyclopentadiene ligand. A vibrational analysis for jet-cooled CaCp has been completed [61] and rotationally-resolved spectra have also been reported [62]. Monomethyl-substituted analogues, for example  $CaC_5H_4CH_3$  (CaMeCp), have also been observed, as have monopyrrolates,  $CaC_4H_4N$  (CaPy), in which one of the CH groups is replaced by N [61, 64]. Both CaMeCp and CaPy were found to have the metal atom bonded to the face of the ring. FCFs have been measured for these species, with results that look promising for photon cycling, i.e. diagonal  $0_0^0$  FCF > 0.8 (see Tab. III). Even in these large, complex species,  $\sim 100$  photons or more could be cycled with only a few lasers (see Sec. II B). These species represent a versatile playground for organometallic chemistry due to the possibility of synthesizing species with unique substituents around the ring. Laser cooling of AE-bonded hydrocarbon rings, followed by bond-selective dissociation, represents a plausible way to generate samples of isolated, cold carbon rings. This method is particularly well-suited to hydrocarbons which possess neither electric nor magnetic dipole moments (or very small ones) and are therefore difficult to manipulate in the gas phase in their natural form.

## E. Astrochemistry

Many dozens of molecules have now been identified in circumstellar and interstellar environments [130, 131]. These environments are characterized by a wide range of density and radiation conditions which directly influence the abundances and distribution of these molecules. Many of the molecules proposed in this work (e.g., thiols, alcohols, and hydrocarbons) would provide stringent tests of calculated rate constants used in models to describe astrophysical evolution [130–132]. Laser cooling followed by bond-selective dissociation would provide direct access to many of these species, already trapped at cold/ ultracold temperatures. Ultracold molecules will allow long-lived trapping, increasing the measurement precision, and full internal state control, allowing specific states to be populated in order to generate internal rotational/ vibrational temperatures matching the astrophysically relevant scale of 10s to 100s of K. For example, optical cycling will enable the preparation of state distributions for tailored studies of dynamics and rate coefficients necessary to develop comprehensive models of circumstellar and interstellar evolution. [133, 134].

## F. Surfaces Functionalized for Optical Cycling

It has been proposed recently [135] to functionalize surfaces by depositing an optical cycling center on a substrate while sufficiently decoupling the electronic transition from vibrational leakages. This would permit highly scalable quantum devices, e.g. by patterning 2D arrays of cycling centers in close proximity on a substrate or placing these cycling centers in photonic cavities. The strong couplings and individual addressability in such a platform would allow for applications in biophysics, quantum information processing, many-body dynamics, and quantum optics [135–137]. The ideal “linker” molecule for attaching optical cycling centers to surfaces is far from certain. Our work shows that AE-nitrogen, AE-sulfur, and AE-carbon ring bonds are favorable for optical cycling, complementing the AE-oxygen bond long recognized for its cycling properties. Self-assembled monolayers with a variety of different surface chemistry have been explored, including OH,  $NH_2$ , and COOH [136]. Our present work signals that a wider variety of metal-ligand bonds than previously envisioned may permit photon cycling. Although this research direction remains highly speculative, it can benefit from our suggestion that a more diverse class of AE-ligand bonds can give rise to favorable optical cycling properties.

## V. CONCLUSION

In this paper, we analyze how the discrete breakdown of structural symmetry in polyatomic molecules

influences repeated optical cycling and direct laser cooling – the two cornerstones of modern atomic physics and its vast applications. Despite complications due to the reduced symmetry, we show that for a generic class of asymmetric top molecules optical cycling and laser cooling are possible. Our calculations, combining semi-empirical and *ab initio* methods, demonstrate that a wide array of metal-ligand bonds have favorable optical cycling properties, introducing nitrogen- and sulfur-containing asymmetric compounds as laser cooling candidates. We also discuss how some of the approximations used in these calculations may break down, while showing that this should not significantly hamper the optical cycling possibilities. The experimental outlook is quite bright, thanks in part to the ability to produce large numbers of these molecules in cryogenic buffer-gas beam sources. Finally, we outlined many potential applications of optical cycling and laser cooling of asymmetric top molecules; these spanned a broad range of disciplines from chemistry and surface science to quantum simulation and quantum information processing. Our hope is that this work will spur robust theoretical and experimental exploration, similar to early proposals on diatomic molecules with optical cycling centers. Ultracold asymmetric top molecules represent an exciting development at the intersection of physics and chemistry.

Additional work is necessary to complement the calculations presented here. In particular, improved experimental measurements of the vibrational branching ratios in these species would further benchmark our calculations. Measurements accurate to the  $10^{-3}$  level or better will be necessary to assess the viability of laser cooling for any given species. This level of accuracy is possible with current spectroscopic techniques [138]. Improved theoretical calculations can also aid searches for species suited to laser cooling. *Ab initio* methods have previously been applied to develop a rational basis for molecule selection for linear species [31]. Extensions to non-linear, asymmetric species are now desirable.

*Note* – During the course of manuscript preparation we became aware of a related and complementary work by Klos and Kotochigova [45], where they used *ab initio* methods to calculate Franck-Condon factors for various polyatomic molecules with increasing complexity.

## VI. ACKNOWLEDGMENTS

We gratefully acknowledge Timothy Steimle for his comments on this manuscript and for enthusiastically sharing his knowledge of molecular spectroscopy over many years. We thank Zack Lasner, Louis Baum, Wes Campbell, and Justin Caram for useful discussions. Work at both Harvard and Columbia has been supported by the W. M. Keck Foundation and at Harvard by the Department of Energy. BLA acknowledges support from the NSF GRFP. IK was supported by the Simons Junior Fellow Award.

## Appendix A: Born-Oppenheimer Approximation Breakdown

We have generally been working within the Born-Oppenheimer (BO) approximation, in which potential energy surfaces are assumed to be well-separated and non-interacting. In reality, vibronic coupling between these adiabatic surfaces can affect this picture [139]. BO approximation breakdown is especially likely as the size of the molecule grows because the number of states and the probability of near-degeneracies increases. Furthermore, breakdown of the BO approximation is far more likely in the excited electronic states  $\tilde{A}$ ,  $\tilde{B}$ , and  $\tilde{C}$  due to their close proximity.

BO approximation breakdown can alter the intensities of rovibronic decays as compared to those calculated above. This is not necessarily detrimental to photon cycling and laser cooling, so long as the branching induced by vibronic coupling is contained within a small number of modes which are easily repumped. Whether this is the case will require a careful, specialized analysis for any given molecule of interest. Here, we outline general features of such analyses.

The effects of vibronic coupling can be described by introducing a term,  $H_{ev}$ , to the Hamiltonian which mixes two (unperturbed) electronic states due to the influence of vibrations. It is natural to expand this perturbation term in the normal coordinates, yielding to first order [140]

$$H_{ev}(x, Q) = H_{ev}^0(x, 0) + \sum_j \left( \frac{\partial H_{ev}}{\partial Q_j} \right)_0 Q_j, \quad (\text{A1})$$

where  $x$  are the electronic coordinates and  $Q_j$  the vibrational normal modes. The physical content of Eq. A1 is that vibronic perturbations can be introduced due to direct coupling between two vibronic states (the 0<sup>th</sup> order term) or by a vibrational “promoter” mode (the 1<sup>st</sup> order term).

Because the Hamiltonian belongs to the totally symmetric representation, there are restrictions on which vibronic levels can interact under the influence of Eq. A1. For instance, because  $H_{ev}^0(x, 0)$  is totally symmetric, it can connect the  $\tilde{A}^2A'$  and  $\tilde{C}^2A'$  states in  $C_s$  symmetry. It cannot connect any of the three lowest electronically excited states ( $\tilde{A}^2B_2$ ,  $\tilde{B}^2B_1$ , and  $\tilde{C}^2A_1$ ) in  $C_{2v}$  symmetry because all three of these states have different symmetry.

The 1<sup>st</sup> order term in Eq. A1 is a linear sum over the normal modes, so we consider each term in the sum individually. The product  $\left( \frac{\partial H_{ev}}{\partial Q_j} \right)_0 Q_j$  must be totally symmetric, so the symmetry of  $\left( \frac{\partial H_{ev}}{\partial Q_j} \right)_0$  can be determined once the normal mode symmetries are known. As an example, in  $C_{2v}$  a vibrational mode with symmetry  $b_2$  can induce coupling between vibronic states with symmetries  $A_2$  and  $B_1$ .

While these considerations can help predict the *propensity* for BO approximation breakdown, they do not provide any estimate of the breakdown’s *magnitude*. A simple estimate for the impact of BO approximation breakdown can come from the case of linear molecules which have been previously laser cooled. Typical perturbation matrix elements are in the range of  $\sim 0.5 - 5 \text{ cm}^{-1}$  for CaOH or SrOH when Renner-Teller vibronic interactions are considered [2, 141]. Taking this scale as the typical matrix element, the strength of vibronic interactions can be estimated using second order perturbation theory and typical energy splittings in the excited electronic states. Such splittings are typically  $\sim 100 - 1000 \text{ cm}^{-1}$ , implying that BO breakdown can induce unexpected decays at the  $10^{-3} - 10^{-6}$  level. In the case of very near degeneracies or enhanced coupling matrix elements this interaction can be much stronger.

### Appendix B: Details of *ab initio* calculations

*Ab initio* calculations were performed using the ORCA quantum chemistry program [84]. Molecular orbitals, optimized geometries, normal modes and vibrational frequencies for all the ground and excited states were calculated at the level of unrestricted Kohn-Sham (UKS) DFT using the B3LYP functional in the ORCA package with def2-TZVPP basis following other similar works [28, 142]. The calculations for the excited states used TDDFT. Table V provides a comparison of our calculations for the lowest three electronic excitations with the experimentally measured values. Our agreement is comparable with other reported *ab initio* calculations for such species [143–145]. Tables VI, VII, VIII, and IX provide optimized geometries for the first excited state as well as predicted transition dipole moments for CaSH and CaNH<sub>2</sub>.

### Appendix C: Rotational Structure

The rotational Hamiltonian for an ATM in the principal axis system, including the spin-orbit interaction, can be expressed as [49, 148]

Molecule	Calc. 1	Calc. 2	Calc. 3	Meas. 1	Meas. 2	Meas. 3
CaOH	16699	16699	18363	15998	15998	18022
CaSH	14812	15212	15431	15381	15859	16075
CaNH <sub>2</sub>	16144	16406	17605	15464	15885	17375

TABLE V. Benchmarking comparison of the *ab initio* predicted and experimentally measured 3 lowest electronic transition energies. Values are provided in  $\text{cm}^{-1}$ . Experimental measurements are obtained from Refs. [50, 146, 147]

Atom	X (Å)	Y (Å)	Z (Å)
Ca	0	-0.045481	-0.062492
S	0	-0.037570	2.538967
H	0	1.364911	2.651461

TABLE VI. Optimized geometry for CaSH in the first excited electronic state. Cartesian coordinates are in Angstroms.

Excited State	Tx (au)	Ty (au)	Tz (au)
1	0.00000	2.25849	-0.02413
2	2.17414	0.00000	0.00000
3	0.00000	0.00540	1.73561

TABLE VII. Calculated transition electric dipole moments in atomic units for CaSH for different electronic states.

$$H = A(N_a - L_a)^2 + B(N_b - L_b)^2 + C(N_c - L_c)^2 + \sum_j \xi \ell_j \cdot \mathbf{s}_j, \quad (\text{C1})$$

where  $\hat{N}$  is the total angular momentum excluding spin,  $\hat{L}$  is the electronic orbital angular momentum,  $\xi$  characterizes the spin-orbit interaction, and the sum over  $j$  includes all electrons in the molecule. Following Refs. [49, 56], Eq. C1 can be reduced to a purely rotational Hamiltonian,

$$H_{\text{rot}} = AN_a^2 + BN_b^2 + CN_c^2, \quad (\text{C2})$$

with perturbations arising from cross terms

$$H' = -2(AN_aL_a + BN_bL_b + CN_cL_c) + \sum_j \xi \ell_j \cdot \mathbf{s}_j. \quad (\text{C3})$$

A Van Vleck transformation produces an effective spin-rotation Hamiltonian [49, 56, 148]

$$H_{\text{sr}} = \frac{1}{2} \sum_{\alpha, \beta} \epsilon_{\alpha\beta} (N_\alpha S_\beta + S_\beta N_\alpha), \quad (\text{C4})$$

Atom	X(Å)	Y(Å)	Z(Å)
Ca	0	0	-0.013610
N	0	0	2.102409
H	0	0.806437	2.718700
H	0	-0.806437	2.718700

TABLE VIII. Optimized geometry for CaNH<sub>2</sub> in the first excited electronic state. Cartesian coordinates are in Angstroms.

Excited State	Tx (au)	Ty (au)	Tz (au)
1	0.00000	-2.30296	0.00000
2	2.11105	0.00000	0.00000
3	0.00000	0.00000	-1.54932

TABLE IX. Calculated transition electric dipole moments in atomic units for  $\text{CaNH}_2$  for different electronic states.

that operates only within a given electronic state. The elements of the spin-rotation tensor,  $\epsilon_{\alpha\beta}$ , contain first-order contributions due to direct coupling between electron spin and molecular rotation and second-order contributions due to cross terms with the spin-orbit interaction. These second order contributions are often a large portion of the  $\epsilon_{\alpha\beta}$  components. While  $\epsilon_{\alpha\beta}$  has 9 possible parameters, for molecules with orthorhombic symmetry only the three parameters  $\epsilon_{aa}$ ,  $\epsilon_{bb}$ , and  $\epsilon_{cc}$  are nonzero. The rotational constants are also contaminated by second order contributions, although these are generally smaller in magnitude than the first-order (rigid body rotation) terms. We emphasize that careful deperturbation of the constants is important to assign the accurate geometries necessary for FCF calculations.

For the molecules considered in this paper the hyperfine structure is negligible when the only nuclei with nonzero spin are located multiple bond lengths away from the valence electron. (To date, only spin-0 Ca and Sr nuclei have been used in molecular laser cooling experiments.) If fermionic metals are considered as the optical cycling center, these hyperfine terms must be added and the analysis proceeds as a straightforward extension from that presented in this work. Hyperfine interactions can mix rotational states with selection rules  $\Delta N = \pm 2$ ,  $\Delta F = 0$  [149, 150]. However, these couplings are very weak [150] and have not affected laser cooling of molecules to date.

To compute energies and decay strengths, we construct a numerical representation of the Hamiltonian,  $H = H_{\text{rot}} + H_{\text{sr}}$ , in a Hund’s case (b) symmetric top basis,  $|N, K, S, J, M_J\rangle$ , using matrix elements taken from the literature [148, 151]. Numerical diagonalization yields eigenenergies and eigenstates with a block structure as expected on the basis of symmetry consideration [152]. When  $K_a$  ( $K_c$ ) sets the dominant level structure, the  $K_c$  ( $K_a$ ) label distinguishes the two parity components with a given  $J$ .

Note that  $H_{\text{rot}}$  contains matrix elements with  $\Delta K = \pm 2$  selection rules, although these are still diagonal in  $N$  and may only affect the low- $N$  states of interest to laser cooling through higher order perturbations.  $H_{\text{sr}}$  includes both diagonal ( $\langle NK | H_{\text{sr}} | NK \rangle$ ) and off-diagonal ( $\langle NK | H_{\text{sr}} | NK \pm 2 \rangle$ ,  $\langle NK | H_{\text{sr}} | N - 1, K \rangle$ ,  $\langle NK | H_{\text{sr}} | N - 1, K \pm 2 \rangle$ , and  $\langle NK | H_{\text{sr}} | N, K \pm 1 \rangle$ ) elements. The matrix elements that couple states with  $\Delta K = \pm 2$  scale with  $(\epsilon''_{bb} - \epsilon''_{cc})$  and those with  $\Delta K = \pm 1$  (which vanish for molecules with orthorhombic symmetry) scale with

$(\epsilon_{ab} + \epsilon_{ba})$  [148]. As discussed in App. D both of these are expected to be negligible. The matrix elements that preserve  $K$  but couple rotational states with  $\Delta N = \pm 1$  scale directly with  $\epsilon_{aa}$  and  $\frac{1}{2}(\epsilon_{bb} + \epsilon_{cc})$ . As will be discussed in App. D, these terms are not entirely negligible but likely affect photon scattering only after  $\gtrsim 10^5$  optical cycles.

The eigenstates are most conveniently described by the labels  $N_{K_a K_c}$ , where  $N$  is the rotational quantum number, and  $K_a$  and  $K_c$  are labels which correlate to the projection of  $N$  onto the  $a$  and  $c$  axes in the prolate and oblate symmetric top limits, respectively. When we adopted the example of near-prolate ATMs in Fig. 6, the small moment of inertia along the  $a$ -axis means that levels of different  $K_a$  values are widely spaced, each containing a ladder of  $N$  rotational states. For each  $N$ , there are sublevels split by the spin-rotation interaction as the asymmetry doubling. In general, the spin-rotation splitting grows with increasing  $N$  while for a given  $N$  the asymmetry doubling shrinks rapidly with increasing  $K_a$ . It is straightforward to construct a similar diagram for ATMs with any other value of the Ray’s asymmetry parameter  $\kappa \equiv (2B - A - C) / (A - C)$  although the relative energies will shift. For near-oblate species, the roles of  $K_a$  and  $K_c$  are swapped, but otherwise the conclusions remain the same.

#### Appendix D: Rotational Branches and Closure

Electric dipole selection rules can be determined by symmetry considerations applied to the rovibronic states. In particular, electric dipole transitions must obey the constraint [153]

$$\Gamma'' \otimes \Gamma' \supset \Gamma^*, \quad (\text{D1})$$

where  $\Gamma''$  and  $\Gamma'$  are the symmetries of the rovibronic states involved in the transition, and  $\Gamma^*$  is the electric dipole representation of the molecular symmetry group. General selection rules on the values of  $K_a$  and  $K_c$  can be derived by working in the rotation group  $D_2$ . It is useful to compare the rotational selection rules (see Tab. IV) to the case of symmetric top molecules. Consider first a prolate symmetric top molecule, e.g.  $\text{CaCH}_3$  (see Fig. 4 column 2), in which the  $a$ -axis corresponds to the symmetry axis, and the  $b$ - and  $c$ -axes lie in a plane perpendicular to this. In this case, transitions can be characterized as “parallel” or “perpendicular” depending on whether the transition dipole moment is along the symmetry axis or perpendicular to it. Parallel transitions have the selection rule  $\Delta K = 0$  while perpendicular transitions have the selection rule  $\Delta K = \pm 1$ . As the molecule distorts from symmetric, the equivalence between the  $b$ - and  $c$ -axes is broken. Nonetheless, for a near-prolate symmetric top the  $a$ -type transition is still of approximate “parallel” nature, and the  $a$ -type selection rules in Tab. IV are justified. Similar reasoning provides an intuitive basis for

selection rules in approximately “perpendicular” transitions, as well as for near-oblate tops.

ATMs with  $C_{2v}$  symmetry are expected to follow these patterns rigorously, as the three components of  $\hat{\mu}$  belong to a different irreducible representation of the symmetry group [153]. This is also reflected in the alignment of the principal axes with the electronic orbitals. In the more general case of  $C_s$  symmetry, a given excited state can decay by coupling to one of several components of  $\hat{\mu}$ ; for example, both  $\hat{\mu}_a$  and  $\hat{\mu}_b$  belong to  $A'$ . Geometrically, the transition moments, determined by the electronic wavefunctions, and the principal axes, determined by the geometry of the molecule, are misaligned. This means that either  $K_a$  or  $K_c$ , or both, can change in a generic electronic decay. For example, in CaSH the  $\tilde{C} \rightarrow \tilde{X}$  transition can couple to either  $\hat{\mu}_a$  or  $\hat{\mu}_c$ . In addition, off-diagonal couplings between electronic manifolds due to a term  $((\epsilon_{ab} + \epsilon_{ba})/2)$  in the spin-rotation Hamiltonian can mix the rotational state labels  $K_a$  and  $K_c$ . The magnitude of this effect will vary from species to species depending on the spin-rotation tensor.

A simple estimate for the relative intensity of  $c$ -type transitions to that of  $a$ -type transitions in molecules with  $C_s$  symmetry can be obtained by considering the relative alignment between the principal axes (which determine the rotational structure) and the metal-ligand bond (which determines the local symmetry of the valence orbitals). In the case of molecules like CaSH and SrSH, the angle between the metal-sulfur bond and the  $a$ -axis is typically  $\sim 0.5^\circ$ . This would imply that roughly 1 in  $10^4$  decays from  $\tilde{C} \rightarrow \tilde{X}$  couples to  $\hat{\mu}_c$ . This number is consistent with the transition dipole moments computed by our *ab initio* calculations in Tab. VII, which predict transition strengths that differ by a factor of  $\sim 100$ . This means that, if fewer than  $10^4$  photon scatters are required, laser cooling of CaSH can proceed using only the scheme from a single panel of Fig. 6. To scatter additional photons without population loss, either microwave remixing or additional laser frequency components can be used to repump population which decays due to these small branches.

The effect of state mixing, Eq. C3, is most prominent in the electronically excited states. For example, rotation about the  $a$ -axis can induce mixing between the  $\tilde{A}$  and  $\tilde{B}$  states which will tend to unquench the orbital angular momentum. Ref. [154] provides a physical picture for these interactions: in the non-rotating molecule, the  $\tilde{A}$  and  $\tilde{B}$  states correspond to standing  $p\pi$  orbitals—one along the  $b$ -axis, and one along the  $c$ -axis—with quenched orbital angular momentum. As the molecule begins to rotate, the  $p\pi$  orbitals follow adiabatically, but eventually decouple from the nuclear framework as a net orbital angular momentum  $\langle L_z \rangle$  is induced. This is reflected, for example, in the values of  $\epsilon_{aa}$  measured for the hydrosulfides and monoamides [48, 154]. The magnitude of this interaction grows with increasing  $K_a$  and in the limit of large  $K_a$ ,  $\epsilon_{aa} \rightarrow A_{SO}$ . Similarly, rotation about the  $b$ -axis can lead to interactions between  $\tilde{A}$  and

$\tilde{C}$  states, and rotation about the  $c$ -axis can mix the  $\tilde{B}$  and  $\tilde{C}$  states [49].

Whether, and to what degree, these interactions affect laser cooling will differ from one species to another. Generally speaking, for near-prolate species the interaction between  $\tilde{A}$  and  $\tilde{B}$  states is of little concern, as rotationally closed optical cycles with hybrid  $bc$ -type selection rules differ only by which subset of asymmetry doublet components are driven by the laser (see Fig. 6(b) and (c)). The full set of levels typically covers  $\ll 1$  GHz and can easily be addressed with a single laser. Mixing between the  $\tilde{C}$  state and either of  $\tilde{A}$  or  $\tilde{B}$  introduces bands with selection rule  $\Delta K_a = 0, \pm 1$ , requiring the addition of one additional laser per vibrational band. Alternatively, microwave remixing can be used to return population to the optical cycle. This is very similar to the case of symmetric top molecules [30]. For near-oblate molecules the same ideas apply, though with the role of the  $a$ - and  $c$ -axes reversed. Finally, as the orbital angular momentum of the  $\tilde{A}$  or  $\tilde{C}$  state is unquenched ( $\langle L_z \rangle \rightarrow 1$ ) the level structure will approach that of a  ${}^2\Pi$  state in symmetric species. In such a case, an additional rotational decay to the  $2_{11}, J'' = 3/2$  level may increase in strength. This is analogous to the decay to the  $N = 2, K = 1, J = 3/2$  parity doublet in symmetric top species. As was shown in Ref. [30], this level is straightforward to remix into the optical cycle.

Interactions among the electronically excited states may unquench the electronic orbital angular momentum and induce transitions with  $\Delta N = \pm 2$ . The relative strength of such decays will vary from species to species, and for excited states with spin-rotation constants  $\epsilon_{aa}$  small relative to the spacing between vibronic states levels (as is common) the probability of these decays will approach zero. For instance,  $\epsilon'_{aa}/\Delta E_{\tilde{B}-\tilde{A}} \sim 10^{-2}$  in the molecules CaSH and SrSH [55]. Thus this mixing will likely be relevant once more than  $\sim 3 \times 10^4$  photons are scattered. Note, too, that the  $\Delta N = \pm 2$  rovibronic decay will be induced as the  $\tilde{A}$  and  $\tilde{B}$  states coalesce into the  $\tilde{A}^2E$  state in molecules with near- $C_{3v}$  symmetry. This requires the addition of a laser frequency (or microwave) to repump the  $2_{1K_c}, J'' = 3/2$  state, as discussed in Ref. [30]. Note that this is the same state requiring remixing for reasons already discussed above, i.e. this is not a *new* loss channel.

Off-diagonal terms of the spin-rotation interaction within the ground state may also be relevant.  $H_{sr}$  may mix states that differ by  $\Delta K_a = \pm 2$  and by  $\Delta N = \pm 1$ . For the ATMs proposed here, the  $\Delta K = \pm 2$  terms are proportional to  $(\epsilon''_{bb} - \epsilon''_{cc}) \approx 10^{-4} \text{ cm}^{-1}$  [55]. Compared to the typical spacing between states differing in  $K_a$  by  $\pm 2$  ( $\approx 10\text{--}100 \text{ cm}^{-1}$ ), such terms lead to rotational losses at the  $\lesssim 10^{-8}$  level and are negligible. Similarly, for non-orthorhombic molecules there will be matrix elements of  $H_{sr}$  that can mix states with  $\Delta K = \pm 1$ . Such matrix elements are proportional to  $(\epsilon_{ab} + \epsilon_{ba})/2$  [148], which is typically small ( $\sim 10^{-4} \text{ cm}^{-1}$  in CaSH [55]) compared to the spacing between connected levels. Again, we ex-

pect this to lead to mixings at the  $\sim 10^{-8}$  level, which is largely negligible. The  $\Delta N = \pm 1$  terms in  $H_{sr}$  are potentially more relevant. Mixing of the  $2_{K_a K_c}$  rotational level into the  $1_{K_a K_c}$  ground state is most likely to affect the rotationally closed optical cycles. At first order in perturbation theory, the admixed amplitude will be  $\zeta \sim \epsilon_{\alpha\alpha}/4B_\alpha$ , where  $\alpha = a, b, c$  labels the principal axes. Typical values of  $\zeta \approx 1 - 5 \times 10^{-3}$  [58, 155]. Such mix-

ing will present a relevant loss channel after scattering  $\gtrsim 5 \times 10^4$  photons, more than required for typical laser cooling. If such losses begin to affect the optical cycle, remixing via a single additional laser frequency or microwave transitions can be used to increase the photon budget. Once again, this is the same  $N'' = 2$  state that may require repumping for other reasons, so these laser frequencies may already be present.

- 
- [1] D. J. Gross, “The role of symmetry in fundamental physics,” *Proc. Natl. Acad. Sci.* **93**, 14256–14259 (1996).
- [2] M. Li and J. A. Coxon, “Laser spectroscopy of the CaOH  $\tilde{A} - \tilde{X}(020)(000)$  band: Deperturbation of the Fermi resonance, Renner-Teller, and spinorbit interactions,” *J. Chem. Phys.* **97**, 8961–8969 (1992).
- [3] T. D. Lee and C. N. Yang, “Question of parity conservation in weak interactions,” *Physical Review* **104**, 254–258 (1956).
- [4] M.-A. Bouchiat and C. Bouchiat, “Parity violation in atoms,” *Rep. Prog. Phys.* **60**, 1351–1396 (1997).
- [5] M. Simunovic, J. J. Metzger, F. Etoc, A. Yoney, A. Ruzo, I. Martyn, G. Croft, D. S. You, A. H. Brivanlou, and E. D. Siggia, “A 3D model of a human epiblast reveals BMP4-driven symmetry breaking,” *Nat. Cell Biol.* **21**, 900–910 (2019).
- [6] L. N. Vandenberg and M. Levin, “A unified model for left-right asymmetry? Comparison and synthesis of molecular models of embryonic laterality,” *Dev. Biol.* **379**, 1–15 (2013).
- [7] M. Quack, “How important is parity violation for molecular and biomolecular chirality?” *Angew. Chem.* **41**, 4618–4630 (2002).
- [8] D. G. Blackmond, “The origin of biological homochirality,” *Philos. Trans. R. Soc. B* **366**, 2878–2884 (2011).
- [9] R. V. Krems, “Viewpoint: Ultracold controlled chemistry,” *Physics* **3**, 10 (2010).
- [10] R. V. Krems, “Cold controlled chemistry,” *Phys. Chem. Chem. Phys.* **10**, 4079–4092 (2008).
- [11] N Balakrishnan, “Perspective: Ultracold molecules and the dawn of cold controlled chemistry,” *J. Chem. Phys.* **145**, 150901 (2016).
- [12] L. D. Carr, D. DeMille, R. V. Krems, and J. Ye, “Cold and ultracold molecules: Science, technology and applications,” *New J. Phys.* **11**, 055049 (2009).
- [13] D. DeMille, “Diatomic molecules, a window onto fundamental physics,” *Physics Today* **68**, 34 (2015).
- [14] I. Kozyryev and N. R. Hutzler, “Precision measurement of time-reversal symmetry violation with laser-cooled polyatomic molecules,” *Phys. Rev. Lett.* **119**, 133002 (2017).
- [15] A. Prehn, M. Ibrügger, R. Glöckner, G. Rempe, and M. Zeppenfeld, “Optoelectrical cooling of polar molecules to submillikelvin temperatures,” *Phys. Rev. Lett.* **116**, 063005 (2016).
- [16] J. Barry, D. McCarron, E. Norrgard, M. Steinecker, and D. DeMille, “Magneto-optical trapping of a diatomic molecule,” *Nature* **512**, 286–289 (2014).
- [17] E. B. Norrgard, D. J. McCarron, M. H. Steinecker, M. R. Tarbutt, and D. DeMille, “Submillikelvin dipolar molecules in a radio-frequency magneto-optical trap,” *Phys. Rev. Lett.* **116**, 063004 (2016).
- [18] S. Truppe, H. J. Williams, N. J. Fitch, M. Hambach, T. E. Wall, E. A. Hinds, B. E. Sauer, and M. R. Tarbutt, “An intense, cold, velocity-controlled molecular beam by frequency-chirped laser slowing,” *New J. Phys.* **19**, 022001 (2017).
- [19] S. Truppe, H. J. Williams, M. Hambach, L. Caldwell, N. J. Fitch, E. A. Hinds, B. E. Sauer, and M. R. Tarbutt, “Molecules cooled below the Doppler limit,” *Nat. Phys.* (2017).
- [20] L. Anderegg, B. L. Augenbraun, E. Chae, N. R. Hutzler, A. Ravi, A. L. Collopy, J. Ye, W. Ketterle, and J. M. Doyle, “Radio frequency magneto-optical trapping of CaF with high density,” *Phys. Rev. Lett.* **119**, 103201 (2017).
- [21] L. W. Cheuk, L. Anderegg, B. L. Augenbraun, Y. Bao, S. Burchesky, W. Ketterle, and J. M. Doyle, “ $\Lambda$ -enhanced imaging of molecules in an optical trap,” *Phys. Rev. Lett.* **121**, 083201 (2018).
- [22] A. L. Collopy, S. Ding, Y. Wu, I. A. Finneran, L. Anderegg, B. L. Augenbraun, J. M. Doyle, and J. Ye, “3-D magneto-optical trap of yttrium monoxide,” *Phys. Rev. Lett.* **121**, 213201 (2018).
- [23] I. Kozyryev, L. Baum, K. Matsuda, B. Hemmerling, and J. M. Doyle, “Radiation pressure force from optical cycling on a polyatomic molecule,” *J. Phys. B* **49**, 134002 (2016).
- [24] I. Kozyryev, L. Baum, K. Matsuda, B. L. Augenbraun, L. Anderegg, A. Sedlack, and J. M. Doyle, “Sisyphus laser cooling of a polyatomic molecule,” *Phys. Rev. Lett.* **118**, 173201 (2017).
- [25] B. L. Augenbraun, Z. D. Lasner, A. Frenett, H. Sawaoka, C. Miller, T. C. Steimle, and J. M. Doyle, “Laser-cooled polyatomic molecules for improved electron electric dipole moment searches,” *New J. Phys.* , Accepted (2020).
- [26] L. Baum, D. Mitra, N. Vilas, C. Hallas, B. L. Augenbraun, S. Raval, and J. M. Doyle, “Magneto-optical forces applied to polyatomic molecules,” (In preparation) (2020).
- [27] M. R. Tarbutt, “Laser cooling of molecules,” *Contemp. Phys.* **59**, 356–376 (2018).
- [28] T. Isaev and R. Berger, “Polyatomic candidates for cooling of molecules with lasers from simple theoretical concepts,” *Phys. Rev. Lett.* **116**, 063006 (2016).
- [29] C. T. Scurlock, T. Henderson, S. Bosely, K. Y. Jung, and T. C. Steimle, “Molecular beam optical stark spectroscopy of CaSH,” *J. Chem. Phys.* **100**, 5481–5490 (1994).
- [30] I. Kozyryev, L. Baum, K. Matsuda, and J. M. Doyle, “Proposal for laser cooling of complex poly-

- atomic molecules,” *ChemPhysChem* **17**, 3641 (2016).
- [31] M. V. Ivanov, F. H. Bangerter, and A. I. Krylov, “Towards a rational design of laser-coolable molecules: insights from equation-of-motion coupled-cluster calculations,” *Phys. Chem. Chem. Phys.* **21**, 19447–19457 (2019).
- [32] Daniel McCarron, “Laser cooling and trapping molecules,” *J. Phys. B* **51**, 212001 (2018).
- [33] B. K. Stuhl, B. C. Sawyer, D. Wang, and J. Ye, “Magneto-optical trap for polar molecules,” *Phys. Rev. Lett.* **101**, 243002 (2008).
- [34] A. M. Ellis, “Main group metal-ligand interactions in small molecules: New insights from laser spectroscopy,” *Int. Rev. Phys. Chem.* **20**, 551–590 (2001).
- [35] P. F. Bernath, “Gas-phase inorganic chemistry: Monovalent derivatives of calcium and strontium,” *Science* **254**, 665–670 (1991).
- [36] P. F. Bernath, “Spectroscopy and photochemistry of polyatomic alkaline earth containing molecules,” *Adv. Photochem.* **23**, 1–62 (1997).
- [37] E. S. Shuman, J. F. Barry, D. R. Glenn, and D. DeMille, “Radiative force from optical cycling on a diatomic molecule,” *Phys. Rev. Lett.* **103**, 223001 (2009).
- [38] E. S. Shuman, J. F. Barry, and D. DeMille, “Laser cooling of a diatomic molecule,” *Nature* **467**, 820–823 (2010).
- [39] J. F. Barry, E. S. Shuman, E. B. Norrgard, and D. DeMille, “Laser radiation pressure slowing of a molecular beam,” *Phys. Rev. Lett.* **108**, 103002 (2012).
- [40] D. J. McCarron, E. B. Norrgard, M. H. Steinecker, and D. DeMille, “Improved magneto-optical trapping of a diatomic molecule,” *New J. Phys.* **17**, 035014 (2015).
- [41] M. H. Steinecker, D. J. McCarron, Y. Zhu, and D. DeMille, “Improved radio-frequency magneto-optical trap of SrF molecules,” *ChemPhysChem* **17**, 3664–3669 (2016).
- [42] H. J. Williams, S. Truppe, M. Hambach, L. Caldwell, N. J. Fitch, E. A. Hinds, B. E. Sauer, and M. R. Tarbutt, “Characteristics of a magneto-optical trap of molecules,” *New J. Phys.* **19**, 113035 (2017).
- [43] L. Caldwell, J. A. Devlin, H. J. Williams, N. J. Fitch, E. A. Hinds, B. E. Sauer, and M. R. Tarbutt, “Deep laser cooling and efficient magnetic compression of molecules,” *Phys. Rev. Lett.* **123**, 033202 (2019).
- [44] J. Lim, J. R. Almond, M. A. Trigatzis, J. A. Devlin, N. J. Fitch, B. E. Sauer, M. R. Tarbutt, and E. A. Hinds, “Laser cooled YbF molecules for measuring the electron’s electric dipole moment,” *Phys. Rev. Lett.* **120**, 123201 (2018).
- [45] Jacek Kłos and Svetlana Kotochigova, “Prospects for laser cooling of polyatomic molecules with increasing complexity,” (2019), [arXiv:1912.09364](https://arxiv.org/abs/1912.09364).
- [46] A. J. Marr, M. Tanimoto, D. Goodridge, and T. C. Steimle, “A study of the  $\tilde{A}^2B_2 - \tilde{X}^2A_1$  band system of CaNH<sub>2</sub> employing molecular beam optical Stark spectroscopy,” *J. Chem. Phys.* **103**, 4466–4475 (1995).
- [47] Z. Morbi, C. Zhao, J. W. Hepburn, and P. F. Bernath, “High-resolution visible laser spectroscopy of the  $\tilde{B}^2B_1 - \tilde{X}^2A_1$  transition of CaNH<sub>2</sub>,” *J. of Chem. Phys.* **108**, 8891–8898 (1998).
- [48] C. R. Brazier and P. F. Bernath, “High-Resolution Laser Spectroscopy of the  $\tilde{A}^2B_2 - \tilde{X}^2A_1$  and  $\tilde{B}^2B_1 - \tilde{X}^2A_1$  Systems of SrNH<sub>2</sub>,” *J. Mol. Spec.* **201**, 116–123 (2000).
- [49] Z. Morbi, C. Zhao, and P. F. Bernath, “A high-resolution analysis of the  $\tilde{C}^2A_1 - \tilde{X}^2A_1$  transition of CaNH<sub>2</sub>: Pure precession in polyatomic molecules,” *J. Chem. Phys.* **106**, 4860–4868 (1997).
- [50] P. M. Sheridan, M. J. Dick, J.-G. Wang, and P. F. Bernath, “Rotational analysis of the  $\tilde{C}^2A_1 - \tilde{X}^2A_1$  transition of SrNH<sub>2</sub>,” *J. Mol. Spec.* **233**, 269–274 (2005).
- [51] P. M. Sheridan and L. M. Ziurys, “Laboratory Detection of the MgNH<sub>2</sub> Radical ( $\tilde{X}^2A_1$ ),” *Astrophys. J.* **540**, L61–L64 (2000).
- [52] P. M. Sheridan and L. M. Ziurys, “Trends in the alkaline-earth amide series: The millimetre-wave spectrum of MgNH<sub>2</sub> and MgND<sub>2</sub> ( $^2A_1$ ),” *Can. J. Phys.* **79**, 409–421 (2001).
- [53] R. F. Wormsbecher, M. Trkula, C. Martner, R. E. Penn, and D. O. Harris, “Chemiluminescent reactions of alkaline-earth metals with water and hydrazine,” *J. Mol. Spec.* **97**, 29–36 (1983).
- [54] C. N. Jarman and P. F. Bernath, “A high-resolution analysis of the  $\tilde{A}^2A' - \tilde{X}^2A'$  transition of CaSH by laser excitation spectroscopy,” *J. Chem. Phys.* **98**, 6697–6703 (1993).
- [55] P. M. Sheridan, M. J. Dick, J.-G. Wang, P. F. Bernath, and P. M. Sheridan, “High-resolution investigation of the excited electronic states of CaSH and SrSH by laser excitation spectroscopy,” *Mol. Phys.* **105**, 569–583 (2007).
- [56] J. Shirley, C. Scurlock, T. Steimle, B. Simard, M. Vasseur, and P. A. Hackett, “Molecular beam optical Stark spectroscopy of CaSH,” *J. Chem. Phys.* **93**, 8580–8585 (1990).
- [57] A. Taleb-Bendiab and D. Chomiak, “Millimeter-wave spectrum of MgSH,” *Chem. Phys. Lett.* **334**, 195–199 (2001).
- [58] A. Janczyk and L. M. Ziurys, “Studies of metal hydrosulfides III: The millimeter/submillimeter spectrum of BaSH ( $\tilde{X}^2A'$ ),” *J. Chem. Phys.* **119**, 10702–10712 (2003).
- [59] A. C. Paul, Md. A. Reza, and J. Liu, “Dispersed-fluorescence spectroscopy of jet-cooled calcium ethoxide radical (CaOC<sub>2</sub>H<sub>5</sub>),” *J. Mol. Spec.* **330**, 142–146 (2016).
- [60] A. M. R. P. Bopegedera, W. T. M. L. Fernando, and P. F. Bernath, “Gas-phase inorganic chemistry: laser spectroscopy of calcium and strontium monopyrrolate molecules,” *J. Phys. Chem.* **94**, 4476–4479 (1990).
- [61] E. S. J. Robles, A. M. Ellis, and T. A. Miller, “Electronic spectroscopy of jet-cooled half-sandwich organometallic complexes CaC<sub>5</sub>H<sub>5</sub>, CaC<sub>5</sub>H<sub>4</sub>CH<sub>3</sub>, and CaC<sub>4</sub>H<sub>4</sub>N,” *J. Am. Chem. Soc.* **114**, 7171–7183 (1992).
- [62] T. M. Cerny, J. M. Williamson, and T. A. Miller, “Rotationally resolved electronic spectra of the “half-sandwich” organometallic radical, CaC<sub>5</sub>H<sub>5</sub>,” *J. Chem. Phys.* **102**, 2372–2378 (1995).
- [63] W. T. M. L. Fernando, R. S. Ram, L. C. O’Brien, and P. F. Bernath, “Gas-phase inorganic chemistry: laser spectroscopy of calcium and strontium monothiolates and monohydrosulfides,” *J. Phys. Chem.* **95**, 2665–2668 (1991).
- [64] A. M. R. P. Bopegedera, C. R. Brazier, and P. F. Bernath, “Laser spectroscopy of strontium and calcium monoalkylamides,” *J. Phys. Chem.* **91**, 2779–2781 (1987).
- [65] C. R. Brazier, L. C. Ellingboe, S. Kinsey-Nielsen, and

- P. F. Bernath, "Laser spectroscopy of alkaline earth monoalkoxide free radicals," *J. Am. Chem. Soc.* **108**, 2126–2132 (1986).
- [66] P. M. Sheridan, M. J. Dick, J.-G. Wang, and P. F. Bernath, "High-resolution spectroscopic investigation of the  $\tilde{B}^2A_1 - \tilde{X}^2A_1$  transitions of  $\text{CaCH}_3$  and  $\text{SrCH}_3$ ," *J. Phys. Chem. A* **109**, 10547–10553 (2005).
- [67] A. P. Salzberg, B. E. Applegate, and T. A. Miller, "Rovibronic Spectroscopy of  $\text{MgCH}_3 \tilde{A}^2E \leftarrow \tilde{X}^2A_1$  Transition," *J. Mol. Spec.* **193**, 434–441 (1999).
- [68] R. Rubino, J. M. Williamson, and T. A. Miller, "High resolution electronic spectroscopy of  $\text{MgCH}_3$ ," *J. Chem. Phys.* **103**, 5964–5969 (1995).
- [69] L. C. O'Brien, C. R. Brazier, and P. F. Bernath, "High-resolution laser spectroscopy of strontium monomethoxide,  $\text{SrOCH}_3$ ," *J. Mol. Spec.* **130** (1988).
- [70] MolView, <http://www.molview.org> (2019).
- [71] B. S. D. R. Vamhindi and M. Nsangou, "Accurate *ab initio* potential energy curves and spectroscopic properties of the low-lying electronic states of OH- and SH-molecular anions," *Mol. Phys.* **114**, 2204–2216 (2016).
- [72] Eunmi Chae, *Laser slowing of CaF molecules and progress towards a dual-MOT for Li and CaF*, Ph.D. thesis, Harvard University, Cambridge, MA (2015).
- [73] I. Kozyryev, T. C. Steimle, P. Yu, D.-T. Nguyen, and J. M. Doyle, "Determination of  $\text{CaOH}$  and  $\text{CaOCH}_3$  vibrational branching ratios for direct laser cooling and trapping," *New J. Phys.* **21** (2019).
- [74] D.-T. Nguyen, T. C. Steimle, I. Kozyryev, M. Huang, and A. B. McCoy, "Fluorescence branching ratios and magnetic tuning of the visible spectrum of  $\text{SrOH}$ ," *J. Mol. Spec.* **347**, 7–18 (2018).
- [75] T. A. Isaev, A. V. Zaitsevskii, and E. Eliav, "Laser-coolable polyatomic molecules with heavy nuclei," *J. Phys. B* **50**, 225101 (2017).
- [76] P. Chen, "Photoelectron spectroscopy of reactive intermediates," in *Unimolecular and Biomolecular Reaction Dynamics*, edited by C. Y. Ng, T. Baer, and I. Powis (Wiley, New York, 1994).
- [77] E. Bright Wilson, J. C. Decius, and Paul C. Cross, *Molecular Vibrations: The Theory of Infrared and Raman Vibrational Spectra* (Dover, 1980).
- [78] T. E. Sharp and H. M. Rosenstock, "Franck-Condon Factors for Polyatomic Molecules," *J. Chem. Phys.* **41**, 3453–3463 (1964).
- [79] M. D. Oberlander, *Laser excited fluorescence studies of reactions of group 2 metals with oxygen containing molecules and of heavy group 15 clusters with fluorine: Reactivities, product state distributions, and spectroscopy of the  $\text{BiF } A0+ - X0+$  transition*, Ph.D. thesis, The Ohio State University (1995).
- [80] J. Weber and G. Hohlneicher, "Franck-Condon factors for polyatomic molecules," *Mol. Phys.* **101**, 2125–2144 (2003).
- [81] J. M. Thompsen, P. M. Sheridan, and L. M. Ziurys, "Rotational spectroscopy of the  $\text{SrNH}_2$  and  $\text{SrND}_2$  radicals ( $\tilde{X}^2A_1$ )," *Chem. Phys. Lett.* **330**, 373–382 (2000).
- [82] R. W. Nicholls, "Franck-Condon factor formulae for astrophysical and other molecules," *Astrophys. J. Supplement Series* **47**, 279 (1981).
- [83] R. R. Wright and T. A. Miller, "High-resolution, rotationally resolved electronic spectroscopy of the  $\text{MgNC}$  radical," *J. Mol. Spec.* **194**, 219–228 (1999).
- [84] F. Neese, "The ORCA program system," *Wiley Interdiscip. Rev. Comput. Mol. Sci.* **2**, 73–78 (2012).
- [85] V. A. Mozhaykiy and A. I. Krylov, "ezspectrum 3.0," [iopenshell.usc.edu/downloads/ezspectrum/](http://iopenshell.usc.edu/downloads/ezspectrum/). (2009).
- [86] H. Kupka and P. H. Cribb, "Multidimensional Franck-Condon integrals and Duschinsky mixing effects," *J. Chem. Phys.* **85**, 1303–1315 (1986).
- [87] P. C. Cross, R. M. Hainer, and G. W. King, "The asymmetric rotor II. calculation of dipole intensities and line classification," *J. Chem. Phys.* **12**, 210–243 (1944).
- [88] G. Herzberg, *Molecular Spectra and Molecular Structure: Electronic Spectra and Electronic Structure of Polyatomic Molecules*, Vol. 3 (Van Nostrand, 1966).
- [89] N. Wells and I. C. Lane, "Prospects for ultracold carbon via charge exchange reactions and laser cooled carbides," *Phys. Chem. Chem. Phys.* **13**, 19036 (2011).
- [90] M. Yeo, M. T. Hummon, A. L. Collopy, B. Yan, B. Hemmerling, E. Chae, J. M. Doyle, and J. Ye, "Rotational state microwave mixing for laser cooling of complex diatomic molecules," *Physical Review Letters* **114** (2015), 10.1103/physrevlett.114.223003.
- [91] S. Truppe, S. Marx, S. Kray, M. Doppelbauer, S. Hofsäss, H. C. Schewe, N. Walter, J. Pérez-Ríos, B. G. Sartakov, and G. Meijer, "Spectroscopic characterization of aluminum monofluoride with relevance to laser cooling and trapping," *Phys. Rev. A* **100**, 052513 (2019).
- [92] L. R. Hunter, S. K. Peck, A. S. Greenspon, S. Saad Alam, and D. DeMille, "Prospects for laser cooling TlF," *Phys. Rev. A* **85**, 012511 (2012).
- [93] R. J. Hendricks, D. A. Holland, S. Truppe, B. E. Sauer, and M. R. Tarbutt, "Vibrational branching ratios and hyperfine structure of  $^{11}\text{BH}$  and its suitability for laser cooling," *Front. Phys.* **2**, 51 (2014).
- [94] N. R. Hutzler, H.-I. Lu, and J. M. Doyle, "The buffer gas beam: An intense, cold, and slow source for atoms and molecules," *Chem. Rev.* **112**, 4803–4827 (2012).
- [95] A. Jadbabaie, N. H. Pilgram, J. Klos, S. Kotochigova, and N. R. Hutzler, "Enhanced yield from a cryogenic buffer gas beam source via excited state chemistry," *New J. Phys.*, Accepted (2020).
- [96] D. DeMille, "Searches for new, massive particles with AMO experiments," in *Current Trends in Atomic Physics* (Oxford University Press, 2019) pp. 29–81.
- [97] Zack Lasner and David DeMille, "Statistical sensitivity of phase measurements via laser-induced fluorescence with optical cycling detection," *Phys. Rev. A* **98**, 053823 (2018).
- [98] C. D. Panda *et al.* (ACME Collaboration), "Stimulated Raman adiabatic passage preparation of a coherent superposition of  $\text{ThO } H^3\Delta_1$  states for an improved electron electric-dipole-moment measurement," *Phys. Rev. A* **93**, 052110 (2016).
- [99] I. Kozyryev, L. Baum, L. Aldridge, P. Yu, E. E. Eyler, and J. M. Doyle, "Coherent bichromatic force deflection of molecules," *Phys. Rev. Lett.* **120**, 063205 (2018).
- [100] X. Long, S. S. Yu, A. M. Jayich, and W. C. Campbell, "Suppressed spontaneous emission for coherent momentum transfer," *Phys. Rev. Lett.* **123**, 033603 (2019).
- [101] S. E. Galica, L. Aldridge, D. J. McCarron, E. E. Eyler, and P. L. Gould, "Deflection of a molecular beam using the bichromatic stimulated force," *Phys. Rev. A* **98**, 023408 (2018).
- [102] N. J. Fitch and M. R. Tarbutt, "Principles and Design of

- a Zeeman-Sisyphus Decelerator for Molecular Beams,” *ChemPhysChem* **17**, 3609–3623 (2016).
- [103] M. R. Tarbutt, “Magneto-optical trapping forces for atoms and molecules with complex level structures,” *New J. Phys.* **17**, 015007 (2015).
- [104] M. L. Wall, K. Maeda, and L. D. Carr, “Simulating quantum magnets with symmetric top molecules,” *Ann. Phys. (Berl.)* **525**, 845–865 (2013).
- [105] M. L. Wall, K. Maeda, and L. D. Carr, “Realizing unconventional quantum magnetism with symmetric top molecules,” *New J. Phys.* **17**, 025001 (2015).
- [106] J. A. Blackmore, L. Caldwell, P. D. Gregory, E. M. Bridge, R. Sawant, J. Aldegunde, J. Mur-Petit, D. Jaksch, J. M. Hutson, B. E. Sauer, M. R. Tarbutt, and S. L. Cornish, “Ultracold molecules for quantum simulation: rotational coherences in CaF and RbCs,” *Quantum Sci. Technol.* **4**, 014010 (2018).
- [107] S. F. Yelin, K. Kirby, and R. Côté, “Schemes for robust quantum computation with polar molecules,” *Phys. Rev. A* **74** (2006).
- [108] P. Yu, L. W. Cheuk, I. Kozryyev, and J. M. Doyle, “A scalable quantum computing platform using symmetric-top molecules,” *New J. Phys.* **21**, 093049 (2019).
- [109] V. V. Albert, J. P. Covey, and J. Preskill, “Robust encoding of a qubit in a molecule,” [arXiv:1911.00099](https://arxiv.org/abs/1911.00099) (2019).
- [110] R. Sawant, J. A. Blackmore, P. D. Gregory, J. Mur-Petit, D. Jaksch, J. Aldegunde, J. M. Hutson, M. R. Tarbutt, and S. L. Cornish, “Ultracold polar molecules as qudits,” *New J. Phys.* (2019).
- [111] Z. Zilic and K. Radecka, “Scaling and Better Approximating Quantum Fourier Transform by Higher Radices,” *IEEE Transactions on Computers* **56**, 202–207 (2007).
- [112] V. Parasa and M. Perkowski, “Quantum phase estimation using multivalued logic,” in *2011 41st IEEE International Symposium on Multiple-Valued Logic* (IEEE, 2011).
- [113] E. T. Campbell, H. Anwar, and D. E. Browne, “Magic-state distillation in all prime dimensions using quantum Reed-Muller codes,” *Phys. Rev. X* **2**, 041021 (2012).
- [114] A. Krishna and J.-P. Tillich, “Towards low overhead magic state distillation,” *Phys. Rev. Lett.* **123**, 070507 (2019).
- [115] D. Patterson, “Method for preparation and readout of polyatomic molecules in single quantum states,” *Phys. Rev. A* **97**, 033403 (2018).
- [116] T. C. Steimle, D. A. Fletcher, K. Y. Jung, and C. T. Scurlock, “A supersonic molecular beam optical Stark study of CaOH and SrOH,” *J. Chem. Phys.* **96**, 2556–2564 (1992).
- [117] M. Härtelt and B. Friedrich, “Directional states of symmetric-top molecules produced by combined static and radiative electric fields,” *J. Chem. Phys.* **128**, 224313 (2008).
- [118] Q. Wei, S. Kais, B. Friedrich, and D. Herschbach, “Entanglement of polar symmetric top molecules as candidate qubits,” *J. Chem. Phys.* **135**, 154102 (2011).
- [119] K. Lin, I. Tutunnikov, J. Qiang, J. Ma, Q. Song, Q. Ji, W. Zhang, H. Li, F. Sun, X. Gong, H. Li, P. Lu, H. Zeng, Y. Prior, I. Sh. Averbukh, and J. Wu, “All-optical field-free three-dimensional orientation of asymmetric-top molecules,” *Nat. Commun.* **9**, 5134 (2018).
- [120] M. S. Safronova, D. Budker, D. DeMille, Derek F. Jackson Kimball, A. Derevianko, and C. W. Clark, “Search for new physics with atoms and molecules,” *Rev. Mod. Phys.* **90**, 025008 (2018).
- [121] P. Jansen, H. L. Bethlem, and W. Ubachs, “Tipping the scales: Search for drifting constants from molecular spectra,” *J. Chem. Phys.* **140**, 010901 (2014).
- [122] M. G. Kozlov and S. A. Levshakov, “Microwave and submillimeter molecular transitions and their dependence on fundamental constants,” *Ann. Phys. (Berl.)* **525**, 452–471 (2013).
- [123] P. Jansen, I. Kleiner, C. Meng, R. M. Lees, M. H. M. Janssen, W. Ubachs, and H. L. Bethlem, “Prospects for high-resolution microwave spectroscopy of methanol in a Stark-deflected molecular beam,” *Mol. Phys.* **111**, 1923–1930 (2013).
- [124] P. Jansen, L.-H. Xu, I. Kleiner, H. L. Bethlem, and W. Ubachs, “Methyl mercaptan (CH<sub>3</sub>SH) as a probe for variation of the proton-to-electron mass ratio,” *Phys. Rev. A* **87**, 052509 (2013).
- [125] B. H. McGuyer, M. McDonald, G. Z. Iwata, M. G. Tarallo, A. T. Grier, F. Apfelbeck, and T. Zelevinsky, “High-precision spectroscopy of ultracold molecules in an optical lattice,” *New J. Phys.* **17**, 055004 (2015).
- [126] I. C. Lane, “Ultracold fluorine production via Doppler cooled BeF,” *Phys. Chem. Chem. Phys.* **14**, 15078 (2012).
- [127] I. C. Lane, “Production of ultracold hydrogen and deuterium via Doppler-cooled Feshbach molecules,” *Phys. Rev. A* **92**, 022511 (2015).
- [128] C. M. Crudden, J. H. Horton, I. I. Ebraldidze, O. V. Zenkina, A. B. McLean, B. Drevniok, Z. She, H.-B. Kraatz, H. J. Mosey, T. Seki, E. C. Keske, J. D. Leake, A. Rousina-Webb, and G. Wu, “Ultra stable self-assembled monolayers of N-heterocyclic carbenes on gold,” *Nat. Chem.* **6**, 409–414 (2014).
- [129] D. L. Kokkin, R. Zhang, T. C. Steimle, I. A. Wyse, B. W. Pearlman, and T. D. Varberg, “Au-S Bonding Revealed from the Characterization of Diatomic Gold Sulfide, AuS,” *J. Phys. Chem. A* **119**, 11659–11667 (2015).
- [130] E. Herbst and E. F. van Dishoeck, “Complex organic interstellar molecules,” *Annu. Rev. Astron. Astrophys.* **47**, 427–480 (2009).
- [131] S. Kwok, “Complex organics in space from Solar System to distant galaxies,” *Astron. Astrophys. Rev.* **24**, 8 (2016).
- [132] R. J. Pattillo, R. Cieszewski, P. C. Stancil, R. C. Forrey, J. F. Babb, J. F. McCann, and B. M. McLaughlin, “Photodissociation of CS from excited rovibrational levels,” *Astrophys. J.* **858**, 10 (2018).
- [133] A. Faure, K. Szalewicz, and L. Wiesenfeld, “Potential energy surface and rotational cross sections for methyl formate colliding with helium,” *J. Chem. Phys.* **135**, 024301 (2011).
- [134] I. W. M. Smith, “Laboratory astrochemistry: gas-phase processes,” *Annu. Rev. Astron. Astrophys.* **49**, 29–66 (2011).
- [135] C. Zhao, S. Yu, A. Shin, Z. Long, T. Atallah, J. Caram, and W. Campbell, “Molecules functionalized with optical cycling centers,” Proceedings of the American Physical Society, DAMOP, Milwaukee, WI (2019).
- [136] G. K. Toworfe, S. Bhattacharyya, R. J. Composto, C. S. Adams, I. M. Shapiro, and P. Ducheyne, “Effect of functional end groups of silane self-assembled mono-

- layer surfaces on apatite formation, fibronectin adsorption and osteoblast cell function,” *J. Tissue Eng. and Regen. Med.* **3**, 26–36 (2009).
- [137] M. Lessel, O. Bäumchen, M. Klos, H. Hähl, R. Fetzer, M. Paulus, R. Seemann, and K. Jacobs, “Self-assembled silane monolayers: an efficient step-by-step recipe for high-quality, low energy surfaces,” *Surf. Interface Anal.* **47**, 557–564 (2015).
- [138] I. J. Smallman, F. Wang, T. C. Steimle, M. R. Tarbutt, and E. A. Hinds, “Radiative branching ratios for excited states of  $^{174}\text{YbF}$ : Application to laser cooling,” *J. Mol. Spec.* **300**, 3–6 (2014).
- [139] G. Fischer, *Vibronic Coupling: The Interaction between the Electronic and Nuclear Motions* (Academic Press, 1984).
- [140] J. R. Henderson, “ $^1A_2 \leftarrow ^1A_1$  transition of formaldehyde,” *J. Chem. Phys.* **44**, 3496–3500 (1966).
- [141] P. I. Presunka and J. A. Coxon, “Laser spectroscopy of the  $\tilde{A}^2\Pi - \tilde{X}^2\Sigma^+$  transition of SrOH: Deperturbation analysis of Kresonance in the  $v_2 = 1$  level of the  $\tilde{A}^2\Pi$  state,” *J. Chem. Phys.* **101**, 201–222 (1994).
- [142] M. J. O’Rourke and N. R. Hutzler, “Hypermetallic polar molecules for precision measurements,” *Phys Rev A* **100**, 022502 (2019).
- [143] J. V. Ortiz, “Ground and excited states of CaSH through electron propagator calculations,” *Chem. Phys. Lett.* **169**, 116–120 (1990).
- [144] J. Koput and K. A. Peterson, “Ab initio potential energy surface and vibrational-rotational energy levels of  $\tilde{X}^2\Sigma^+$  CaOH,” *J. Phys. Chem. A* **106**, 9595–9599 (2002).
- [145] C. M. Taylor, R. K. Chaudhuri, and K. F. Freed, “Electronic structure of the calcium monohydroxide radical,” *J. Chem. Phys.* **122**, 044317 (2005).
- [146] P. F. Bernath and C. R. Brazier, “Spectroscopy of CaOH,” *Astrophys. J.* **288**, 373–376 (1985).
- [147] M. J. Dick, P. M. Sheridan, J.-G. Wang, S. Yu, and P. F. Bernath, “Optical-optical double resonance spectroscopy of the  $\tilde{D}^2\Sigma^+ - \tilde{A}^2\Pi$  transition of CaOH,” *J. Mol. Spec.* **240**, 238–243 (2006).
- [148] E. Hirota, *High-Resolution Spectroscopy of Transient Molecules* (Springer Berlin Heidelberg, 1985).
- [149] J. M. Brown and A. Carrington, *Rotational spectroscopy of diatomic molecules* (Cambridge Univ. Press, 2003).
- [150] H.-I. Lu, *Magnetic trapping of molecules via optical loading and magnetic slowing*, Ph.D. thesis, Harvard University, Cambridge, MA (2014).
- [151] I. C. Bowater, J. M. Brown, and A. Carrington, “Microwave Spectroscopy of Nonlinear Free Radicals. I. General Theory and Application to the Zeeman Effect in HCO,” *Proc. R. Soc. A* **333**, 265–288 (1973).
- [152] W. Gordy and R. L. Cook, *Microwave molecular spectra* (John Wiley and Sons, 1984).
- [153] P. R. Bunker and P. Jensen, *Molecular symmetry and spectroscopy* (NRC Research Press, 2006).
- [154] C. J. Whitham, B. Soep, J.-P. Visticot, and A. Keller, “Observation and spectroscopy of metallic free radicals produced by reactive collisions during a supersonic expansion,” *J. Chem. Phys.* **93**, 991–1000 (1990).
- [155] M. A. Brewster and L. M. Ziurys, “The pure rotational spectrum of  $\text{CaNH}_2$  and  $\text{CaND}_2$  ( $\tilde{X}^2A_1$ ): Additional proof of planarity,” *J. Chem. Phys.* **113**, 3141–3149 (2000).